# Thermo-mechanical Coil Cooling Model to Tackle Shape and Mechanical Properties Issues after Hot Rolling of Steel Sheets

Daniel Weisz-Patrault, Nicolas Legrand, M Deka, M Magnana, C Cooke, Bertram Ehrhardt, Stéphane Jimenez, Ronan Jacolot

# Thermo-mechanical Coil Cooling Model to Tackle Shape and Mechanical Properties Issues after Hot Rolling of Steel Sheets

**N. Legrand, M. Deka, M. Magana, C. Cooke – ArcelorMittal Global R&D East Chicago, USA**
**B. Ehrhardt – AMNS Calvert[1], USA**
**D. Weisz Patrault – Ecole Polytechnique, France**
**S. Jimenez, R. Jacolot – ArcelorMittal Global R&D, France**

***Abstract:*** *The goal is to better understand the strip shape and hardness variability issues that appear after hot rolling on two distinct high strength steel grades A and B. These issues strongly affect the yield loss of the two grades and are mainly due to late austenite transformation in the coil during its heterogeneous cooling in the coil yard after mandrel removal. To tackle these problems, an existing thermo-mechanical coil cooling model is calibrated on the two grades using industrial temperature measurements of the coils taken with infrared cameras (to tune the coil cooling temperature model) and using laboratory dilatometric tests to tune the phase transformation kinetics model of each grade. The infrared cameras reveal a difference of cooling kinetics between the two grades attributed to a difference of phase transformation kinetics: one grade is mainly coil transforming (grade A) while the other is rather run out table transforming (grade B). This difference was confirmed by the TTT and CCT diagrams established on the two grades with the laboratory dilatometric tests. Furthermore, the calibrated coil cooling model clearly shows that the slow kinetics of coil cooling after mandrel removal depends not only on material parameters, boundary conditions, coil geometry and phase transformation kinetics but also on the heterogeneous contact pressure between laps in the radial direction of the coil. Once calibrated, the model is used to compare the two grades and analyse several new rolling practices to mitigate the issues. Finally the industrial evaluations of some of these new practices are presented together with the yield benefits.*

**KEYWORDS:** HOT ROLLING – COIL COOLING – PHASE TRANSFORMATION – TRANSFORMATION PLASTICITY - RESIDUAL STRESS – SHAPE – HARDNESS VARIABILITY

## INTRODUCTION

### AMNS Calvert finishing mill description

The AMNS Calvert finishing hot strip mill (Alabama, USA) is a 7 stands 4-high mill equiped with bending and CVC on all stands. The run out cooling table has a 151 meters length with a 15,500 $m^3$/hour maximum water cooling capacity and 3 down-coilers (see. figure 1).

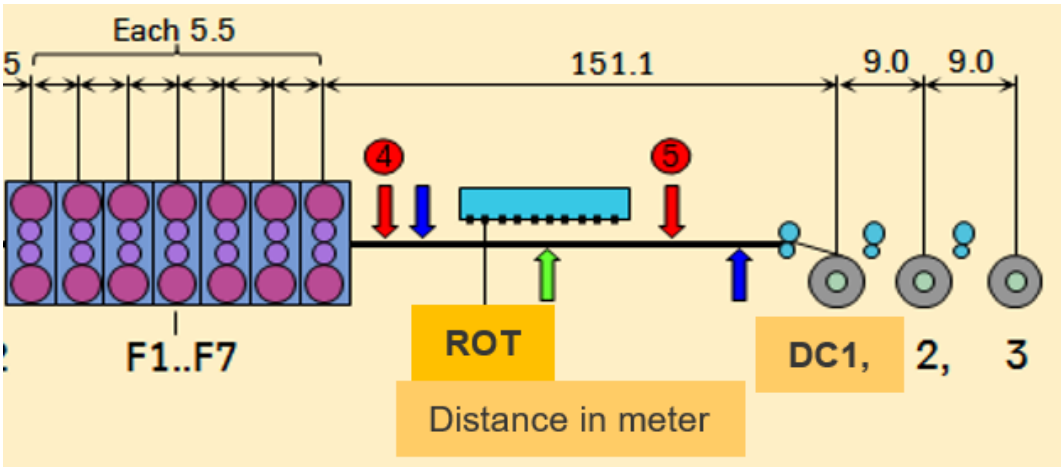


**Fig.1** – AMNS Calvert Finishing Hot Strip Mill layout (ROT: Run Out Table, DC: Down-coiler)

1 **AMNS** Calvert: **A**rcelor**M**ittal-Nippon**S**teel Joint Venture, Alabama, USA

**Industrial problem description**

The Calvert hot strip mill produces two high strength steel grades selected for the study (named grade A and grade B). These grades contain a high amount of Manganese retarding the phase transformation of austenite in the strip when it is cooled down by the Run Out Table (ROT) after hot rolling. Consequently, the remaining austenite at the down-coiler is decomposed by phase transformation later in the coil during its slow and heterogeneous cooling (figure 2). This produces shape and hardness variability issues throughout the coil. These issues are grade dependent and due to thermo-mechanical and metallurgical interactions where the temperature and stress distribution in the coil influence and are being influenced by the transformation. Additionally, during further down cooling at lower temperatures, incomplete austenite decomposition from upper temperatures are being transformed into hard martensitic phases especially at coil extremities (head, tail, edges) because of faster cooling rates. The risk of strip breaks on these hard phases or the risk of slow-down on these shape issues are then considerably increased at the downstream lines, especially in the subsequent cold rolling. Consequently, prior to cold rolling the coils are cropped at their extremities as follows:

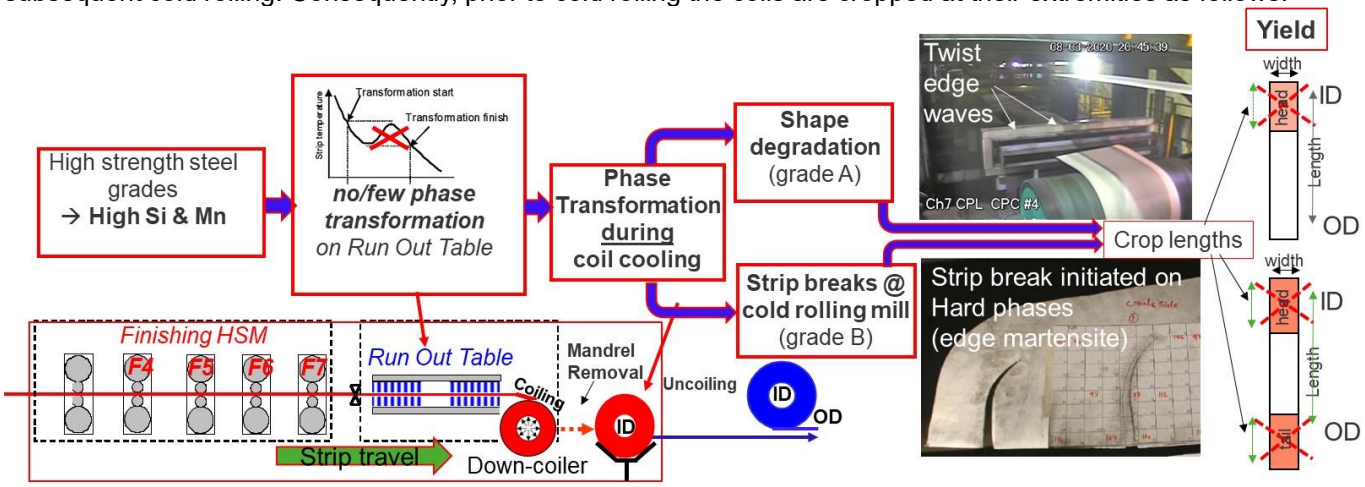


**Fig.2:** Two important sources of yield loss at the Calvert hot rolling mill due to heterogeneous coil cooling: Twist shape issue (grade A) and hard phases formation (grade B) at strip extremities (Inner (ID) and Outer (OD) Diameter).

- **<u>Grade A: twist shape issue</u>**
  It is a complex shape defect with waves in quincunx usually observed after coil cooling for this type of grade [27]: the strip tends to twist around itself while traveling on downstream lines accumulators (see. figure 3). The defect located in hot band coil ID is thus cropped over a certain length. Note that the coil OD does not show any particular twist shape issue so only coil ID is cropped (figure 2). In addition to that croppage, a *batch annealing* prior to cold rolling is made on grade A to soften the hard phases formed during coil cooling at coil extremities (head, tail, edges).

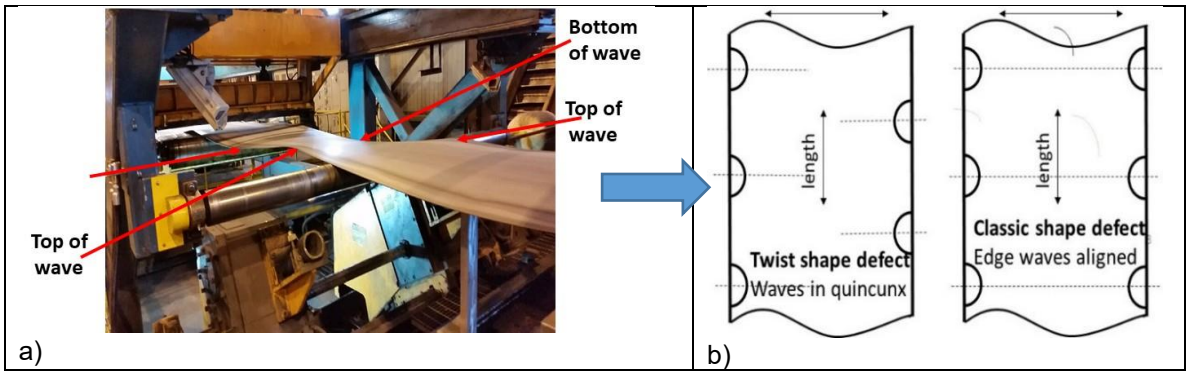


**Fig.3: a)** Twist shape defect observed at a downstream line [27]. **b)** scheme of twist shape defect with edge waves in quincunx, different from a classic wavy edge shape defect with aligned waves

- **<u>Grade B: hardness variability issue</u>**
  The crop length for this grade aims to remove hard phases formed at coil extremities (head, tail and edges) because grade B, in contrast to grade A, does not have any batch annealing prior to cold rolling. It is also highlighted that grade B, in contrast to grade A, does not present twist shape issues.

These crop lengths avoid time losses at downstream lines (strip breaks/slow-down) but create yield loss at hot mill.

**Objectives of the present work**

Based on the above problem description, the primary objective of this work is to minimize the yield loss of the two grades by:

- ***Calibrating an existing coil cooling model to better understand the origin of shape and hardness variability*** issues observed for the two grades and more particularly understand:
  - Why grade A gets severe twist shape issues at coil ID while grade B does not ?
  - Why Twist shape issue of grade A is observed at coil ID only and not at the OD ?
  - Why a batch annealing after hot rolling is required for grade A while it can be avoided for grade B ?
- ***Developing, applying and evaluating some rolling practices*** that can mitigate these issues so that the crop length and associated yield loss of these two grades is reduced.

## EXPERIMENTAL ANALYSIS

### Twist shape issue of grade A: Residual stress characterization

Method: To characterize the residual stresses associated with the twist shape defect of grade A (see. figure 3), sheet samples were collected from 4 different coils (after their cooling) at different distances from coil extreme ID. Cross sections of the coils are 2.5 to 3 mm thickness x ~1100 mm width. Then each sample was cut in the rolling direction in 100 mm width lamellaes using water jet. After cutting, the lamellaes were distorded by the residual stresses release. The magnitude of these distorsions were then measured in I-unit with a 3D scanner Faro X330 to give an estimate of these residual stresses.

Results: Figure 4 presents a sample sheet measured with the scanner before and after cutting in lamellaes and corresponding to coil 480 of table 1.

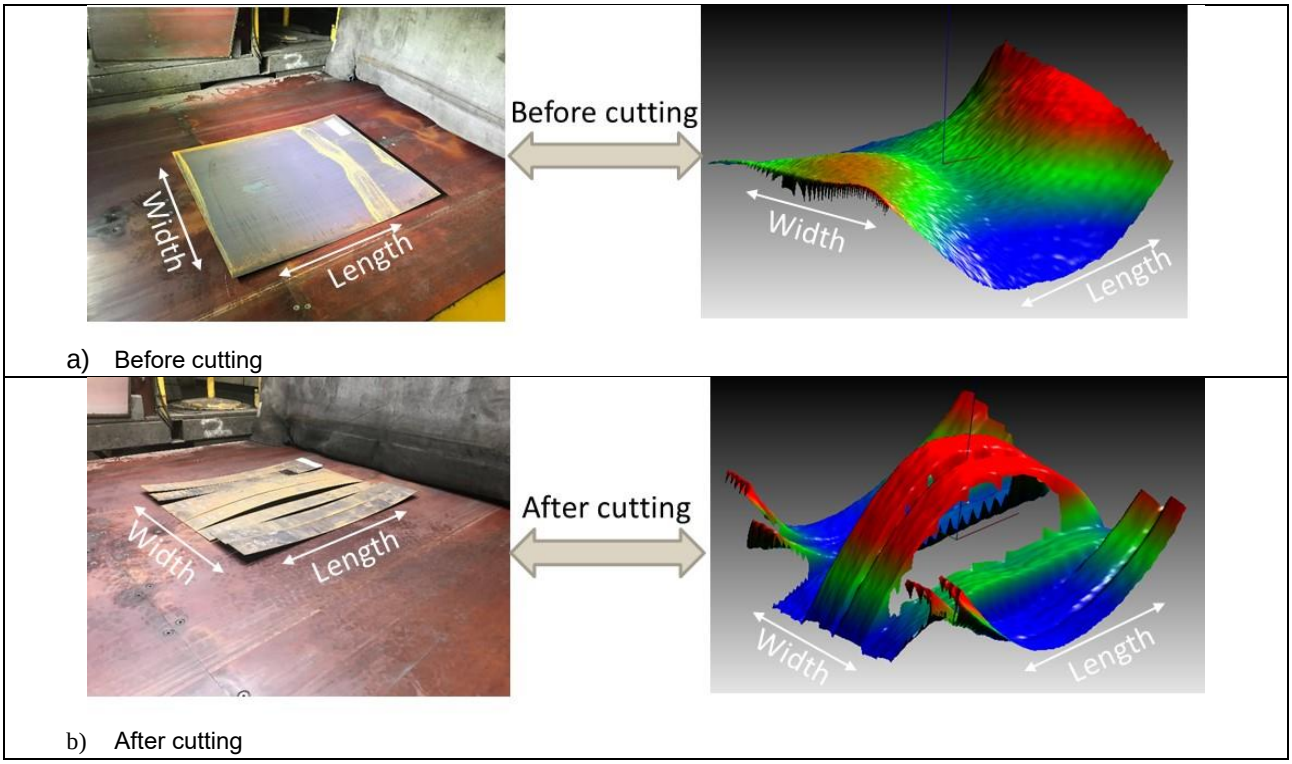


**Fig.4** Twist shape defect in steel sheet sample before and after cutting – coil ID:480XT2 - location 5 meters from coil ID. Left: samples picture – Right: distorded sheets and lamellaes measured by the scanner before and after cutting.

The strong curvature of the lamellaes after cutting suggests some residual stresses distribution within the sheet mainly across thickness (and not across the width as for classic shape defects wavy edges or center buckle which are due to residual stress distribution across the width). This has been confirmed by an additional

experiment (not shown here) where all the lamellaes for each sheet after cutting have been pressed flat on a marble table and their respective measured length was almost the same for all lamellaes. This experiment shows that the curvatures are related to residual stress relaxation across thickness. Moreover, central lamellaes curvature of figure 4 correspond to relaxation of bending stresses that were imposed by the mandrel at down-coiler, while the curvature of edge lamellaes is reversed compared to center. The origin of this reversed curvature in the edges is unclear. Furthermore as shown on table 1, the magnitude of the average distorsions in I-unit are smaller when samples are closer to the mandrel and innermost diameter (5 meters) than at a longer distance (20, 30, 50, 83 meters). This result is counter-intuitive since the closer to the coiler is, the smaller curvature is so the higher bending stresses imposed by the mandrel are. So lamellaes should present higher curvatures when closer to mandrel. This point is discussed further in this paper.

**Table 1**: measured I-units after cutting of twist shape samples and average per sheet sample

| | | coils ID | | | | | | | |
|---|---|---|---|---|---|---|---|---|---|
| | | 490 XT1 | 490 XT2 | 480 XT1 | 480 XT2 | 430 XT1 | 430 XT2 | 440 XT1 | 440 XT2 |
| | distance from ID (meter) | 50 m. | 5 m. | 30 m. | 5 m. | 20 m. | 5 m. | 83 m. | 5 m. |
| lamellaes number | 0 | 614 | 596 | 898 | 191 | 922 | 300 | 163 | 77 |
| | 1 | 294 | 596 | 143 | 104 | 235 | 216 | 248 | 73 |
| | 2 | 871 | 558 | 386 | 9.46 | 353 | 66 | 458 | 9 |
| | 3 | 1097 | 442 | 602 | 353 | 628 | 24 | 582 | 280 |
| | 4 | 1108 | 300 | 609 | 315 | 646 | 16 | 587 | 324 |
| | 5 | 887 | 290 | 419 | 34 | 320 | 24 | 452 | 25 |
| | 6 | 281 | 407 | 171 | 175 | 133 | 14 | 235 | 154 |
| | 7 | 676 | 690 | 416 | 250 | 422 | 90 | 137 | 139 |
| | 8 | - | 575 | - | - | - | | | |
| | **Average I-unit of distorsions** | **729** | **495** | **456** | **179** | **457** | **94** | **358** | **135** |

**Hardness variability issue of grades A and B**

Method: Rockwell C hardness profile measurements were performed across the width on grades A and B samples taken at different distances from coil extremities (coil ID/OD = hot mill coil head/tail). Hardness of grade A was measured only in coil ID, while hardness for grade B was measured both in coil ID and coil OD.

Results: Figures 5 and 6 show hardness measurement results for the two grades. Hardness measurements for grade A (see. figure 5) were made before batch annealing, so hardnesses can be compared between the two grades.

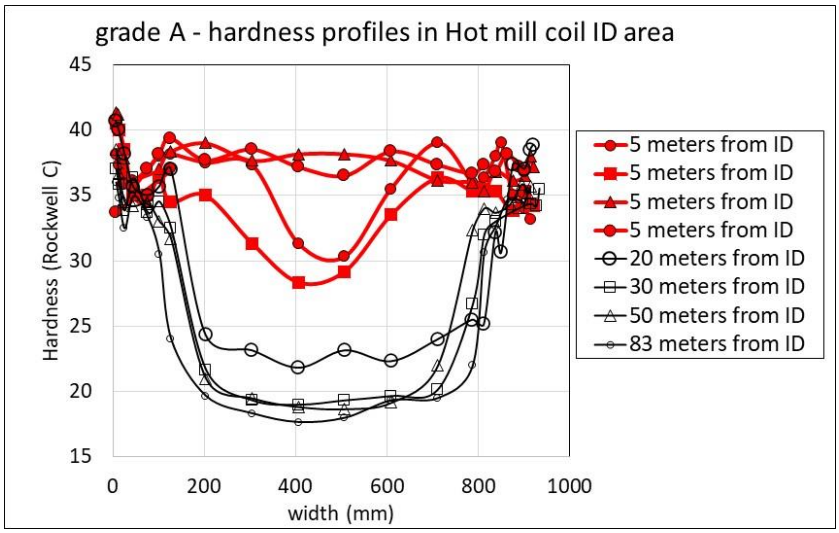


**Fig.5 Grade A:** Hardness profiles across the width at different positions along coil length from coil ID (head) for the 4 samples of table 1 (no measurement made on hot mill coil OD (tail)).

Grade A presents a higher hardness (35-40 HRc: figure 5) in the edges than grade B (25-30 HRc: figure 6). This difference is probably due a higher fraction of hard phases (martensite) in the edges for grade A, which means that grade A has less transformed austenite at coiler than grade B so has more remaining austenite able to transform in martensite in subsequent cooling (in other words grade A is more coil transforming than grade B). This difference of transformation between the two grades is confirmed later in this paper by dilatometric tests, industrial trials and simulation analysis. Moreover grade A samples located close to coil ID (5 meters) have a more homogeneous hardness across the width than at a longer distance (figure 5), which suggests a more homogeneous but faster cooling in very first laps of outer coil area. Finally, figure 6 shows for grade B a variation of hardness in the rolling direction that is stronger at coil OD than at coil ID (except for the extreme lap). This is possibly due to a difference of cooling rate between ID (inner laps) and OD (outer laps): coil OD cools down faster than coil ID as confirmed by the industrial results of next section.

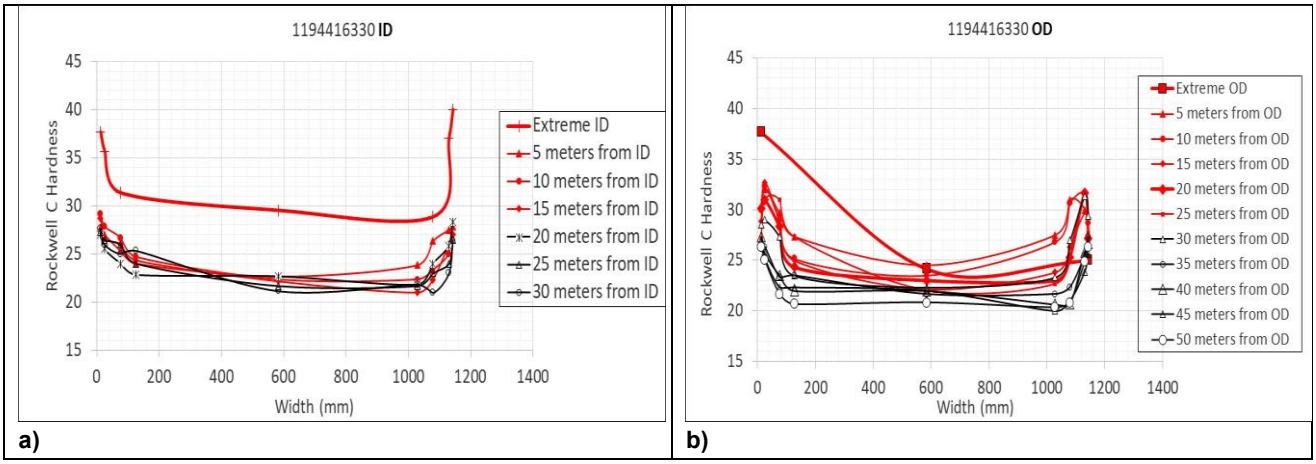


**Fig.6 Grade B:** Hardness profiles across strip width at different positions along coil length
a) at head (HSM coil ID) and b) at tail (HSM coil OD)

### Dilatometric tests on grades A and B: CCT[2], TTT[3] diagrams and influence of austenite plastic deformation in finishing mill

Method: Dilatometric tests were performed on the two grades using a Bahr dilatometer (model 805D) at different cooling rates. The tests conditions are: heating at 10 Celcius/sec till 950 Celcius, then stays 60 seconds at 950 Celcius, then cooling at a constant cooling rate till room temperature. Seven different cooling rates have been used: 0.3, 1.0, 3.0, 10.0, 25.0, 50.0 Celcius/sec.. The samples geometries are cylinders: 10 mm length x 4 mm diameter (for no deformation tests) and 5 mm diameter (for deformation tests). The goal of these dilatometric tests is twofold:

- characterize the transformation kinetics of the grades over a large range of cooling rates that correspond to the industrial conditions, from 20-30 Celcius/sec on the run out table to 0.01-0.005 Celcius/sec in the coil during its slow cooling after mandrel removal.
- Evaluate the possible influence of high temperature plastic deformation in austenite during the finishing hot rolling on the subsequent phase transformation kinetics on the run out cooling table: for that purpose, an initial 20% plastic deformation is applied on the dilatometric sample at high temperature prior to cooling for comparison without deformation.

Results: Figure 7 presents the dilatometric curves during cooling at different cooling rates for the two grades: for low cooling rates (i.e., below 10 Celcius/sec), the ferrite and bainite formations at high temperature is clearly visible for both grades but with higher amount of transformed phases at high temperature for grade B. For higher cooling rates, martensite is formed at MS 300-350 Celcius for both grades.

2 **CCT**: **C**ontinuous **C**ooling **T**ransformation
3 **TTT**: **T**ime **T**emperature **T**ransformation

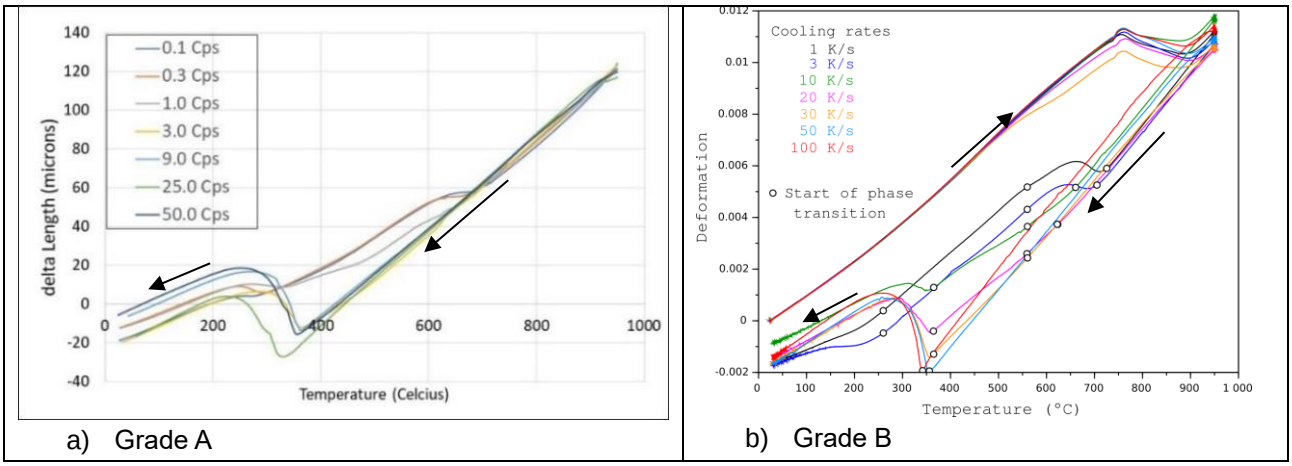


**Fig.7:** Dilatometric tests for different cooling rates and estimated start for each phase transition for grades A and B.

Figure 8 shows the influence of an initial 20% plastic deformation of austenite at 950 celcius prior to cooling: for grade B, this deformation produces a sooner ferrite phase transformation and consequently a decrease of the martensite transformation temperature MS (figure 8-b). Grade A does not present such strong decrease of MS (figure 8-a). This MS shift is thus an evidence that grade B is more sensitive than grade A to austenite plastic deformation during hot rolling to activate high temperature ferrite transformation on the run out table. Consequently, the carbon content in the remaining austenite that transforms into martensite at lower temperatures is higher in grade B (because ferrite formation rejects the carbon in the remaining austenite) than in grade A. This produces the drop of MS for grade B.

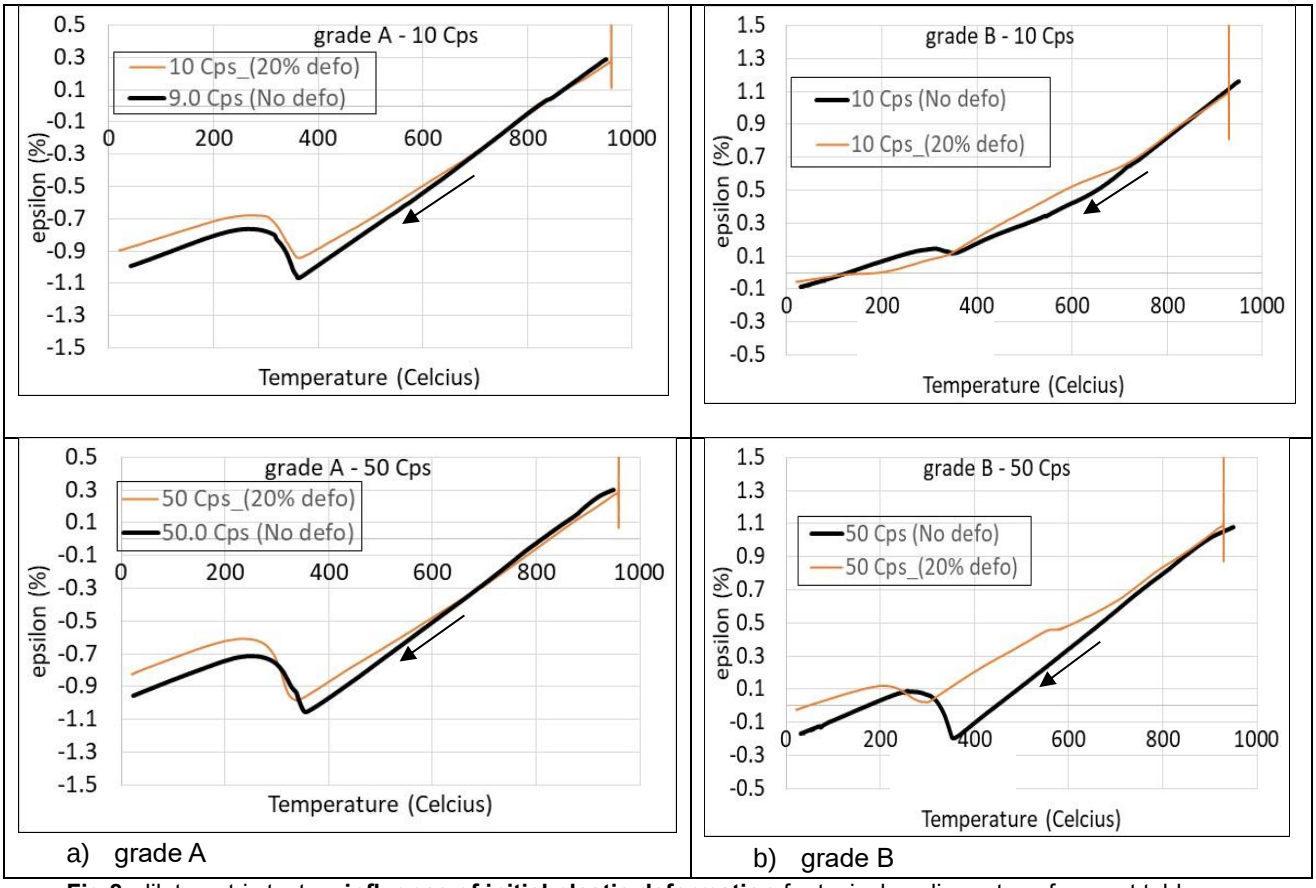


**Fig.8:** dilatometric tests – **influence of initial plastic deformation** for typical cooling rates of run out table

Figure 9 shows the CCT diagrams determined for each grade using dilatometric curves of figure 7 and the phase fractions measured by metallography: both grades form multiple phases (ferrite, bainite, martensite) at

intermediate cooling rates. At higher cooling rates, only martensite is formed while at lower cooling rates pearlite is formed for grade B due to the high amount of carbon content (grade A seems not forming any pearlite at low cooling rates because the carbon content is lower than in grade B). More importantly, grade A shows a later phase transformation start than grade B during cooling: the nose of ferrite start appears at a lower cooling rate for grade A (10 Celcius/sec) compared to grade B (30 Celcius/sec). Finally, grade B presents a strong decrease of MS temperature for low cooling rates (see. figure 9-b) that grade A does not show (see. figure 9-a). This MS decrease is another confirmation of the amount of ferrite formed at high temperature that is higher in grade B than in grade A.

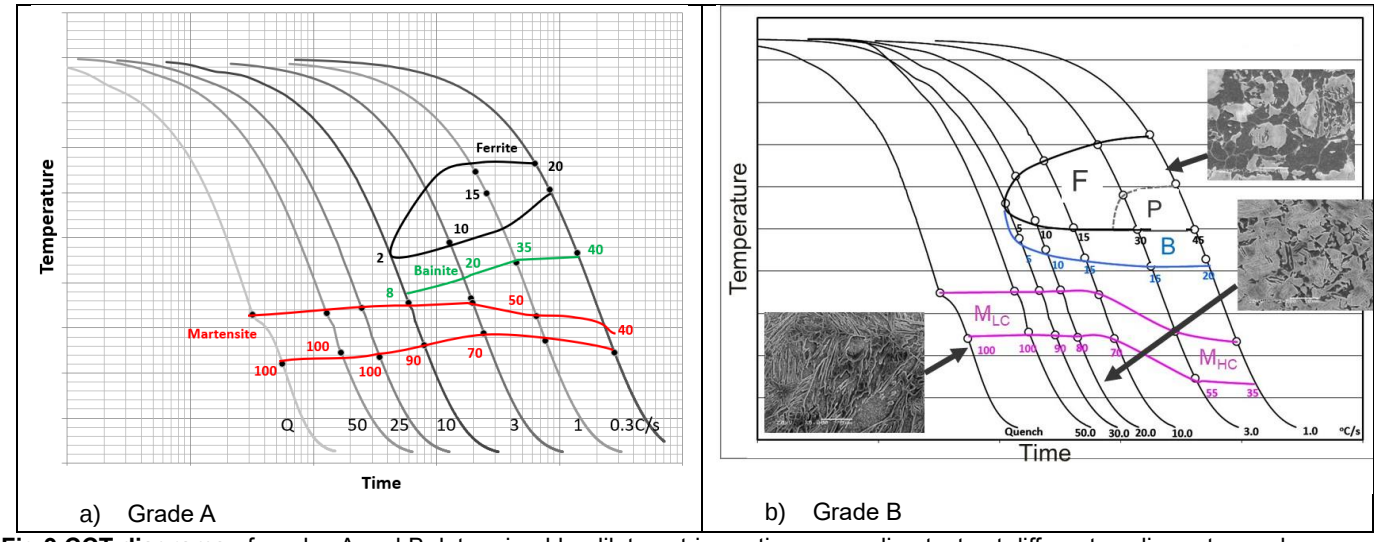


**Fig.9 CCT diagrams** of grades A and B determined by dilatometric continuous cooling tests at different cooling rates and corresponding phase fractions obtained by metallography [26].

Figure 10 shows the TTT diagram determined with isothermal dilatometric tests performed at different temperature plateaus on the two grades: grade A has a long bay (i.e., long delay of transformation) at a specific temperature (figure 10-a), while grade B shows a bay shorter in time than grade A and at a lower temperature than grade A. These results confirm again that grade A has a much slower transformation than grade B.

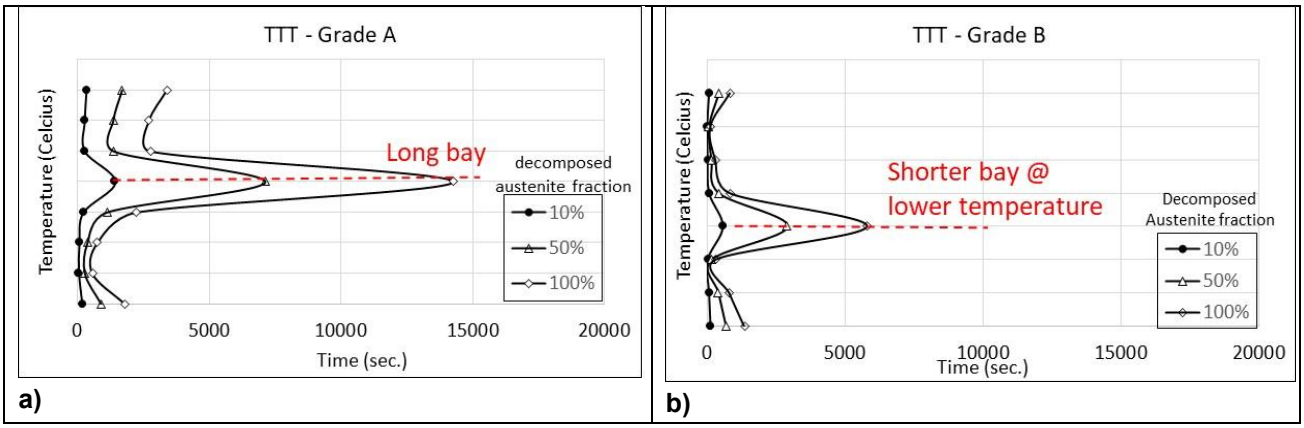


**Fig.10 TTT diagrams** (estimate) determined by isothermal dilatometric tests: a) grade A and b) grade B (phase fractions roughly estimated with the dilatometric curves, no metallography was made here) – linear time scale.

**Industrial coil cooling trials with infrared cameras**

Trials conditions: Measurements of coil temperature evolution during cooling after hot rolling and mandrel removal were made on 3 different coils using infrared cameras: coil 1 (grade B) and coils 2 and 3 (grade A). Figure 11 presents the location of the 3 cameras with respect to the 3 coils: two different cameras measured temperature respectively of the front and of the side of coil 1 (grade B). A third camera measured temperature of the front of the two other coils 2 and 3 (grade A). To get absolute temperature measurements from the

infrared cameras, the emissivity of the cameras was fixed to 0.84, value corresponding to high temperature steel emissivity.

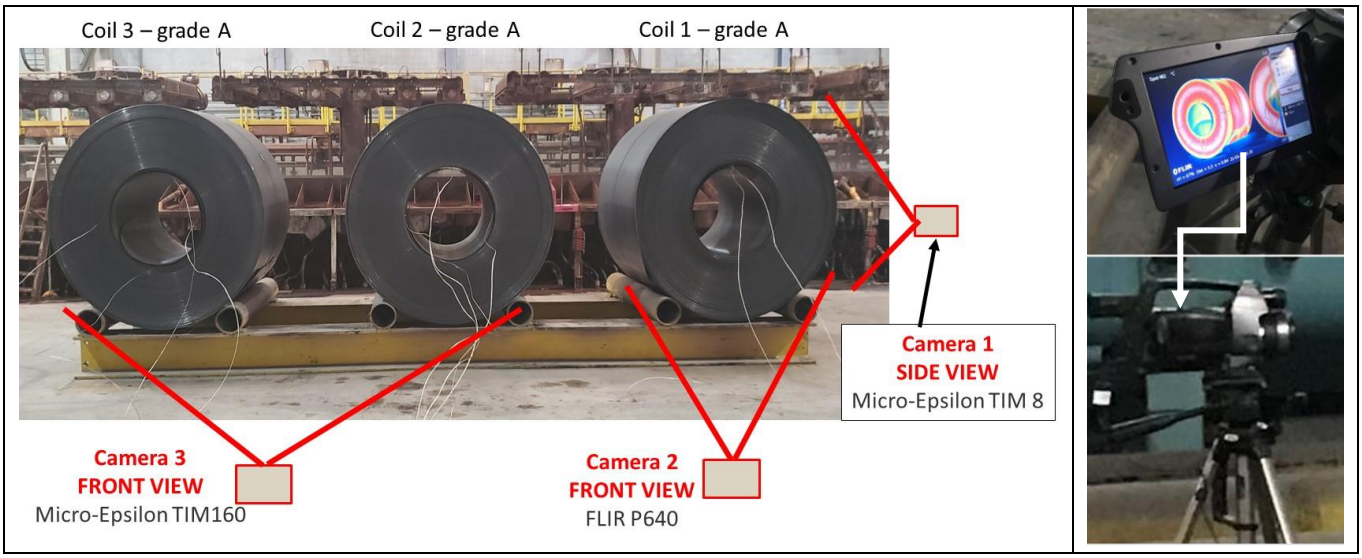


**Fig.11** 3 coils cooling trial at finishing mill exit, near the down-coiler and infrared cameras location. Coils dimensions (thickness (mm) x width (mm) x length (meter): coil1: 2.92x1181x642 - coil2: 2.98x1163x636 coil3: 2.98x1169x635

Trials results: Figure 12 presents the temperature measurements from the FLIR infrared camera for coil 3 at three different times of cooling after mandrel removal. These measurements reveal three important results:

- Central laps in the front view (coil body) stay significantly warmer than the rest of the coil (white areas).
- Corners of the coil (inner and outer laps) cool down faster than the rest of the coil.
- Coil temperature is rather axi-symetric all along the cooling time (influence of neighbour coils seems negligible.

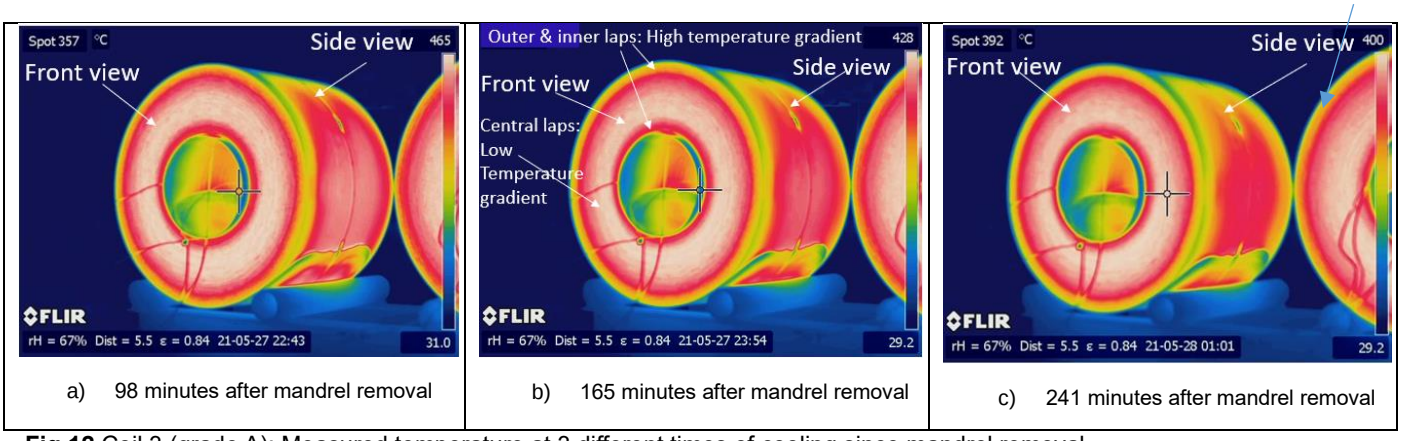


a) 98 minutes after mandrel removal

b) 165 minutes after mandrel removal

c) 241 minutes after mandrel removal

**Fig.12** Coil 3 (grade A): Measured temperature at 3 different times of cooling since mandrel removal

Figure 13 presents the temperature measured on coil 2 (grade A) on front view respectively in inner, central and outer laps: the central laps show a clear 100 Celcius re-increase of temperature during coil cooling with a peak of temperature at 500 Celcius, approximately 45 min after mandrel removal. Note that inner and outer laps do not present such a re-increase. This peak of temperature is attributed to a late phase transformation in the coil that generates heat: it is probably the austenite to bainite transition according to the CCT diagram on figure 9-a. Figure 13 shows also that at the beginning of coil cooling, inner laps (green) are colder than outer laps (blue) and of course colder than the central laps (red). Then during further cooling, inner laps cool down more slowly than outer laps and become warmer at the end of cooling (~50 Celcius difference between inner and outer laps). The reason why at early stages of cooling inner laps are colder is due to their contact with the cold mandrel during coiling which tends to cool down faster these laps. In the subsequent cooling, outer laps cool down faster than inner laps because the outer surface of the coil is subjected to radiation and

convection heat exchanges while the inner surface of the coil is in a closer area with less convection and heat losses by radiation possibly tend to be cancelled from each others due to the internal circular surface of the inner lap. This important observation is used to estimate the thermal boundary conditions for the coil cooling model simulations (tables 5 and 6).

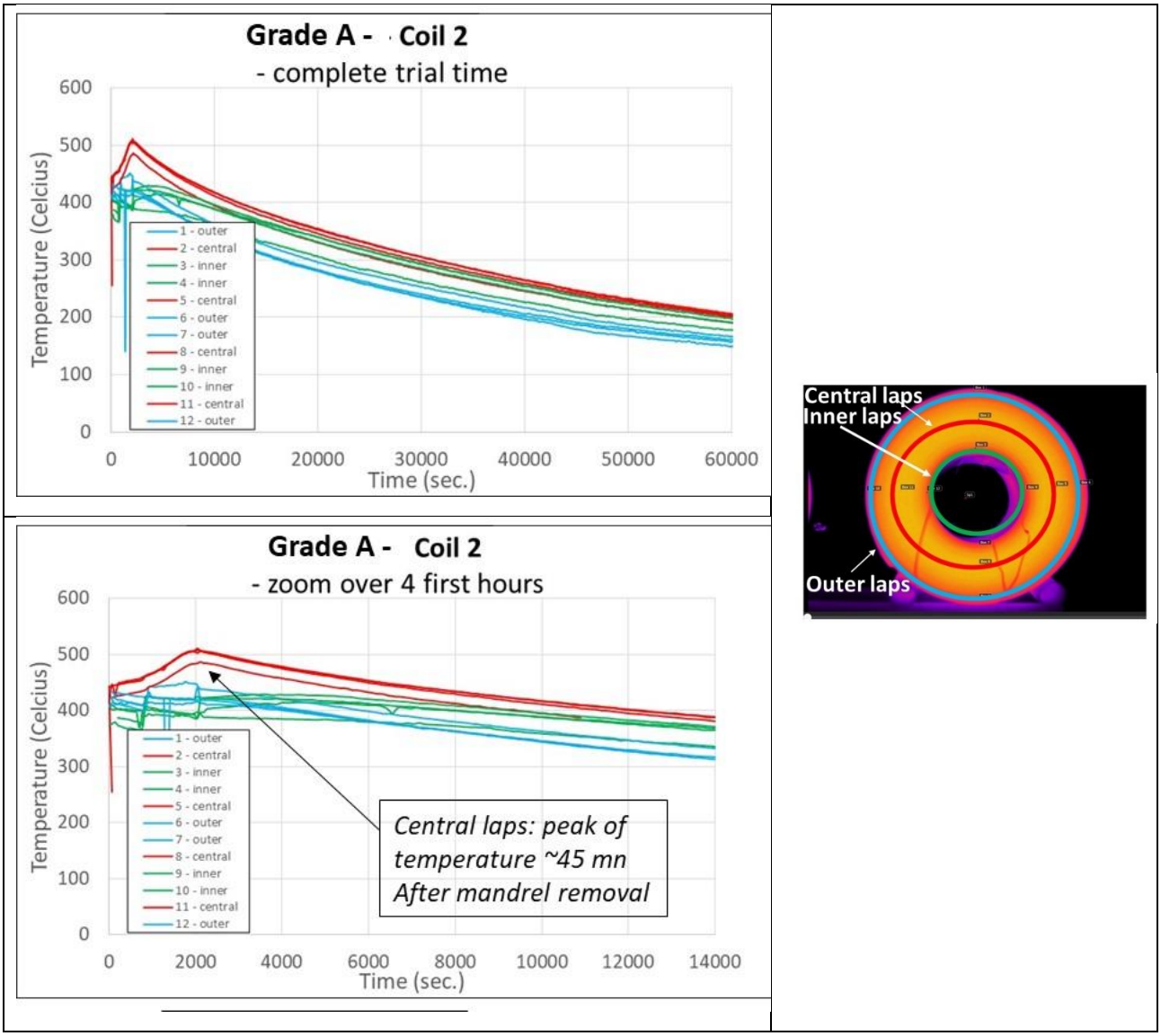


**Fig.13** Coil 2 (grade A): Measured temperature evolution during coil cooling - face view (colors: green, red, blue: inner, central, outer laps).

Figure 14 shows the temperature measured on coil 1 (grade B) with the two cameras respectively on front and side views. In contrast to grade A, the central laps of grade B (coil 1) do not show any re-increase of temperature during coil cooling after mandrel removal (figure 14-c), this is probably due to the fact that grade B has a faster phase transformation than grade A (figures 7 and 8), so has more austenite already transformed on the run out table, so less to transform in the coil. Moreover, figure 14 shows also that the central laps (front view) stay significantly warmer than the outer lap (side view) all along the coil cooling while these two areas are free surfaces of the coil in contact with air so they should cool down similarly. This observation is discussed more in details in the next sections.

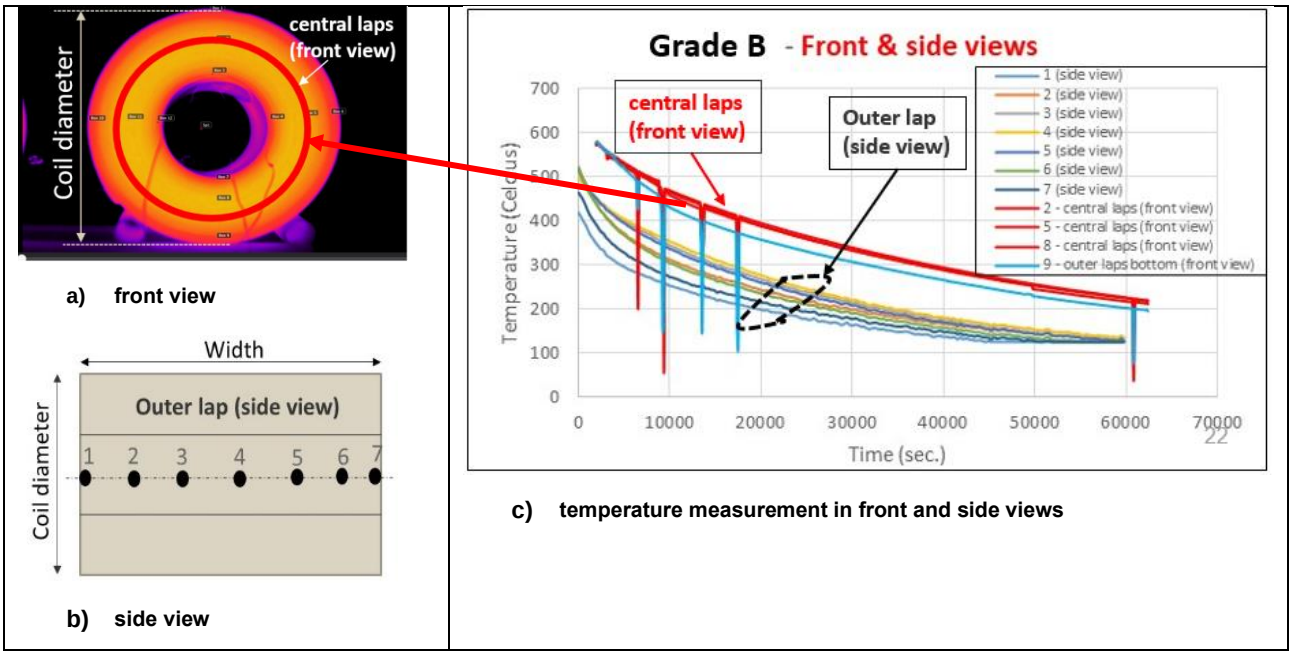


**Fig.14** Coil 1 (grade B): Measured temperature evolution during coil cooling in central laps (front view) and in outer lap (side view: 7 points across the width)

Finally coil temperature in the radial direction (average value at 4 radial positions in the circumference) for different cooling times after mandrel removal (front view) for coil 1 (grade B) is shown on figure 15: as already shown on infrared cameras pictures, all along the coil cooling, important temperature gradients are present in outer and inner laps area while central laps present much smaller gradients.

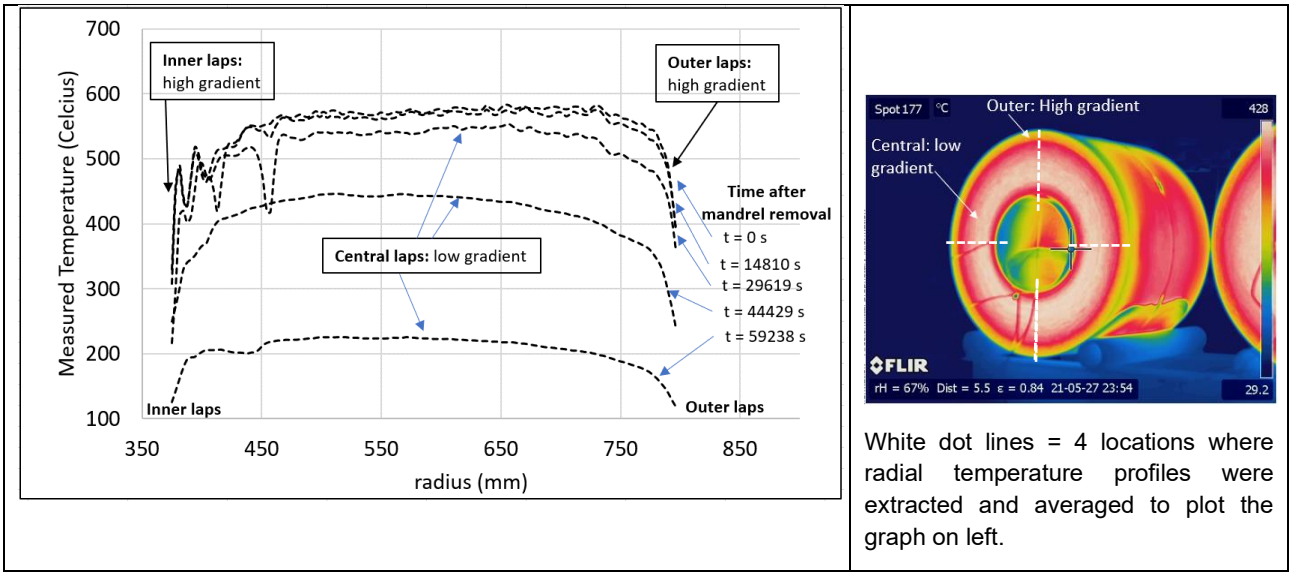


White dot lines = 4 locations where radial temperature profiles were extracted and averaged to plot the graph on left.

**Fig.15** Coil 1 (grade B): a) Measured temperature in the radial direction at 4 different cooling times.

**<u>Important observation concerning air gap between laps</u>:**

Air gap between laps usually exists in the coil due to the strip crown. However, during the cooling trials, it was observed that central laps in the body of the coil were very tight in the edge area with a very small air gap in between (front view) since it was impossible to introduce a thermocouple between laps. While in the inner and outer laps area (coil ID and OD), laps were much looser with possibility to introduce thermocouples.
Moreover, It is believed that this variation of lap contact (tight contact for central laps and loose contact for inner and outer laps) is directly correlated with the temperature profile in the radial direction of the coil (front) as shown on figure 15: important air gap in between inner and outer laps tend to thermally isolate each lap from the others so the temperature gradient through laps is important leading to strong temperature variations in ID and OD areas. While small air gap in between central laps favors a good thermal contact between laps

that produces small temperature gradients (i.e., plateaus) through laps. This important observation is used in the modeling section (figure 20) to estimate a more realistic inter-lap pressure in the radial direction of the coil. Figure 16 proposes two possible mechanisms that could create higher air gap and loose contact for respectively inner and outer laps favoring the corresponding radial temperature profile of figure 15:

- **Mechanism 1**: the pressure applied by the band belt on the outer lap in the center of the coil tends to create a flexion of outer laps edges leading to less contact between laps in the edge area.
- **Mechanism 2**: the temperature gradient in the radial direction in the edge of the coil (front view) in outer and inner area produces a phenomenon of deflection of each lap in these areas because of temperature gradient through lap thickness: deflection up for outer laps, deflection down for inner laps (because the temperature gradient has opposite direction between inner and outer laps).

These two mechanisms are only assumptions, their real influence need to be verified by simulation.

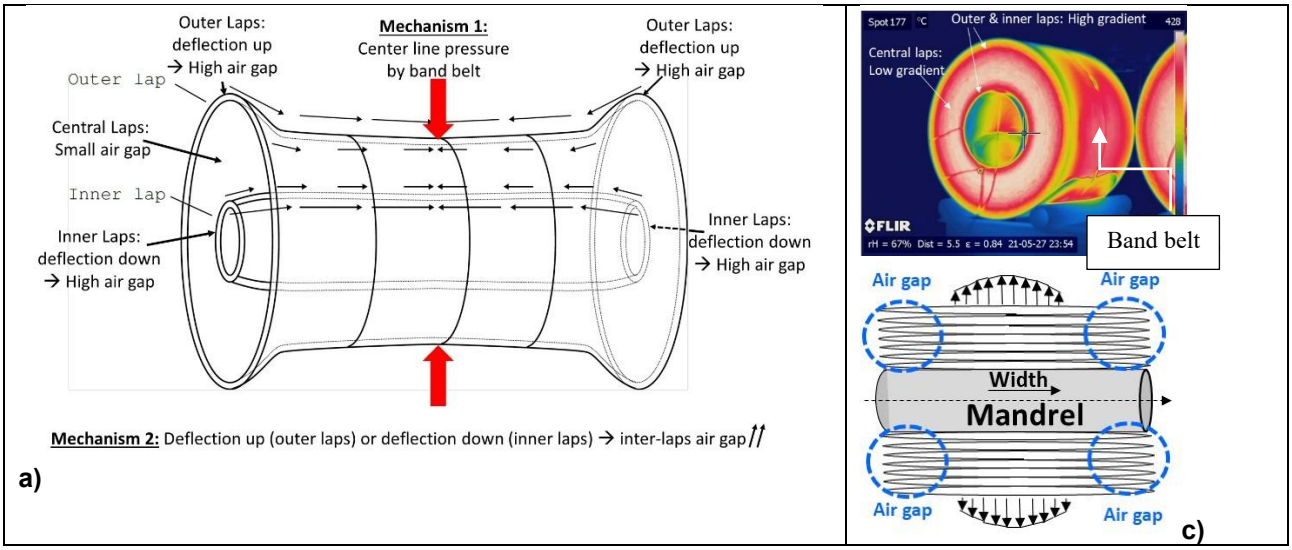


**Fig.16** a) the two possible mechanisms responsible for the higher air-gap in inner and outer laps during coil cooling. b) Relationship air gaps with temperature gradients across the laps. c) air gap in the coil due to stacking laps.

## THERMO-MECHANICAL COIL COOLING MODEL

Among numerous numerical methods [1], a series of relatively fast numerical models covering rolling process [2], run out table [3], [4], [5], [6] and coiling and coil cooling [7], [8], [9], [10], [11], [12] have been developed to predict temperature field history, phase proportions and residual stresses in steel sheets. Such models along with contact stress [13], [14], [15], heat flux [16], [17], [18], [19], [20] and flatness measurements [21] are developed to better understand and control the effect of process parameter on product quality. However, these models need to be calibrated on the studied grades to accurately predict temperature kinetics, phase transitions and residual stress evolution, which depend on thermal expansion, phase transition volume change, and transformation induced plasticity [22].

### Avrami and Koistinen models for phase transformation kinetics

In this contribution, diffusive phase transitions (i.e., austenite to ferrite, pearlite and bainite) are modeled via Avrami equations [23], displacive austenite to martensite phase transition is modeled by Koistinen law [24]. The dilatometric tests at the different cooling rates (figure 7) are exploited here in a new method to calibrate simple Avrami and Koistinen transformation equations to predict transformation kinetics of the two grades.

Standard lever rule method:

The main difficulty with the two grades is that several phase transitions successively take place during each cooling rate, which makes difficult the quantification of the transformed phase fraction for each phase by using only the dilatometric curves and the classic lever rule method. Indeed, uncertainties may be high when the amount of phase fraction to be identified by the lever rule method is low. Moreover, the lever rule method is limited to the identification of the decomposed austenite fraction without distinguishing the new phases formed.

Alternative method to lever rule:

To overcome the above difficulties, a method detailed below and based on [22] was developed:

- Rough estimate of the amount of each transformed phase for each dilatometric curve using final phase fraction determined by metallography on dilatometric samples.
- Estimate the thermal expansion coefficients for each phase using dilatometric curves.
- Estimate successive phase transitions (i.e. austenite to ferrite + pearlite, bainite and martensite) by integrating the measured strain over time using the following equation (where the sum is taken over all the product phases, $\varepsilon$ is the measured strain,$X_j$ the phase proportion of the $j$th phase, $T$ the temperature,$\alpha_j$ thermal expansion coefficients, and $\rho_j$the densities):

$$\dot{\varepsilon} = \sum_j \frac{1}{3}\left(\frac{\rho_{austenite}}{\rho_j} - 1\right)\dot{X}_j + \left(\alpha_{austenite} + \sum X_j\left(\alpha_j - \alpha_{austenite}\right)\right)\dot{T} \qquad [1]$$

The dilatometric curves of figure 7 with the estimated start of each phase transition are used for phase transition model tuning on grades A and B. The density ratios between product phases and austenite are involved in this equation and must be estimated as well. They have been estimated by best fitting the final phase proportions. Higher cooling rates are associated with more martensite while lower cooling rates are associated with more ferrite + pearlite and bainite. Therefore density ratios have been estimated for martensite by fitting with high cooling rates (i.e., 100, 50, 30 and 20 Celcius / s) while ferrite + pearlite and bainite density ratios have been identified on lower cooling rates (i.e., 1, 3 and 10 Celcius/s). As a result the final phase proportions estimated by analyzing micrographs of final microstructures are best fitted for high cooling rates for martensite and for lower cooling rates for ferrite+pearlite and bainite. On this basis, the phase fraction of each phase for each cooling rate is inferred. Simple isothermal Avrami equations are used because measurements uncertainties are not negligible so that it would be difficult to identify non isothermal Avrami equations that require to identify more parameters. Hence the phase proportion is written in the following form ($X_{austenite}^{residual}$: remaining austenite,$k_j$and $n_j$: Avrami coefficients and $t$: time):

$$X_j = X_{austenite}^{residual}\left(1 - exp\left(-k_j t^{n_j}\right)\right) \qquad [2]$$

In addition for martensitic phase transformation a Koistinen law is used instead (i.e., $j = martensite$, $T_{mar}$is the temperature start of martensitic phase transition):

$$X_j = X_{austenite}^{residual}\left(1 - exp\left(-k_j(T - T_{mar})\right)\right) \qquad [3]$$

Coefficients $k_j$and $n_j$are identified by minimizing the distance between measured phase proportions for all cooling rates and the Avrami and Koistinen models.

Results: Final results obtained with this alternative method are presented below:

- Table 2 shows the comparison between predicted and measured phase fractions: Ferrite+Pearlite is rather well estimated for low cooling rates (i.e., 1 to 10 celcius/s) but is overestimated for higher cooling rates (i.e., 30 to 100 celcius/s), while martensite is underestimated for low cooling rates (i.e., 1 to 3 celcius/s) and high cooling rates (i.e., 50 to 100 celcius/s) because bainite is overestimated.

**Table 2:** Phase proportions estimation from micrograph analysis 1) obtained from the calibrated model 2)

| Phase % | Grade | 0,3 °C/s | | 1 °C/s | | 3 °C/s | | 10 °C/s | | 20 °C/s | | 25 °C/s | | 30 °C/s | | 50 °C/s | | 80 °C/s | |
|---|---|---|---|---|---|---|---|---|---|---|---|---|---|---|---|---|---|---|---|
| | | 1) | 2) | 1) | 2) | 1) | 2) | 1) | 2) | 1) | 2) | 1) | 2) | 1) | 2) | 1) | 2) | 1) | 2) |
| Ferrite+Pearlite | Grade A | 20 | 30 | 15 | 10 | 10 | 30 | 2 | 18 | 0 | 13 | 0 | 0 | X | X | 0 | 8 | 0 | 6 |
| | Grade B | X | X | 45 | 47 | 30 | 30 | 15 | 18 | 10 | 13 | X | X | 5 | 10.5 | 0 | 8 | 0 | 6 |
| Bainite | Grade A | 40 | 32.5 | 35 | 34 | 20 | 27 | 8 | 24 | 0 | 21 | 0 | 20 | X | X | 0 | 4.3 | 0 | 2.5 |
| | Grade B | X | X | 20 | 37 | 15 | 27 | 15 | 14 | 10 | 9 | X | X | 5 | 6.5 | 0 | 4 | 0 | 2.5 |
| Martensite | Grade A | 40 | 37 | 50 | 55.5 | 70 | 42 | 90 | 68 | 100 | 78 | 100 | 80 | X | X | 100 | 87 | 100 | 91 |
| | Grade B | X | X | 35 | 15.5 | 55 | 42 | 70 | 68 | 80 | 78 | X | X | 90 | 82 | 100 | 87 | 100 | 91 |

- Table 3 shows the identification of density ratio for each phase that is required by equation [1].

**Table 3:** Thermal expansion coefficients and density ratios for the different phases (grades A and B)

| Phases | Thermal expansion coefficients | Density ratios |
|---|---|---|
| Austenite | $22.7 \times 10^{-6}$ | 1 |
| Ferrite + Pearlite | $12.7 \times 10^{-6}$ | 0.964 |
| Bainite | $12.7 \times 10^{-6}$ | 0.95 |
| Martensite | $12.0 \times 10^{-6}$ | 0.977 |

- Finally Table 4 presents the Avrami and Koistenen coefficients identified for grade B. These coefficients will be used with the thermomechanical coil cooling model in the next section.

**Table 4:** Avrami and Koistinen coefficients of the phase transition model tuned on grades A and B

| | | **Coefficients** | |
|---|---|---|---|
| **Phases** | **Grades** | $k_j$ | $n_j$ |
| **Ferrite + Pearlite** | Grade A | 0.00076 | 0.9964 |
| | Grade B | 0.047 | 0.51 |
| **Bainite** | Grade A | 0.1459 | 0.23 |
| | Grade B | 0.011 | 0.82 |
| **Martensite** | Grade A | 0.0167 | X |
| | Grade B | 0.023 | X |

**Thermomechanical coil cooling model tuning**

In this section, numerical simulations of coil cooling are performed using the existing thermo-mechanical coil cooling model (figure 17) to be compared with the infrared cameras measurements.

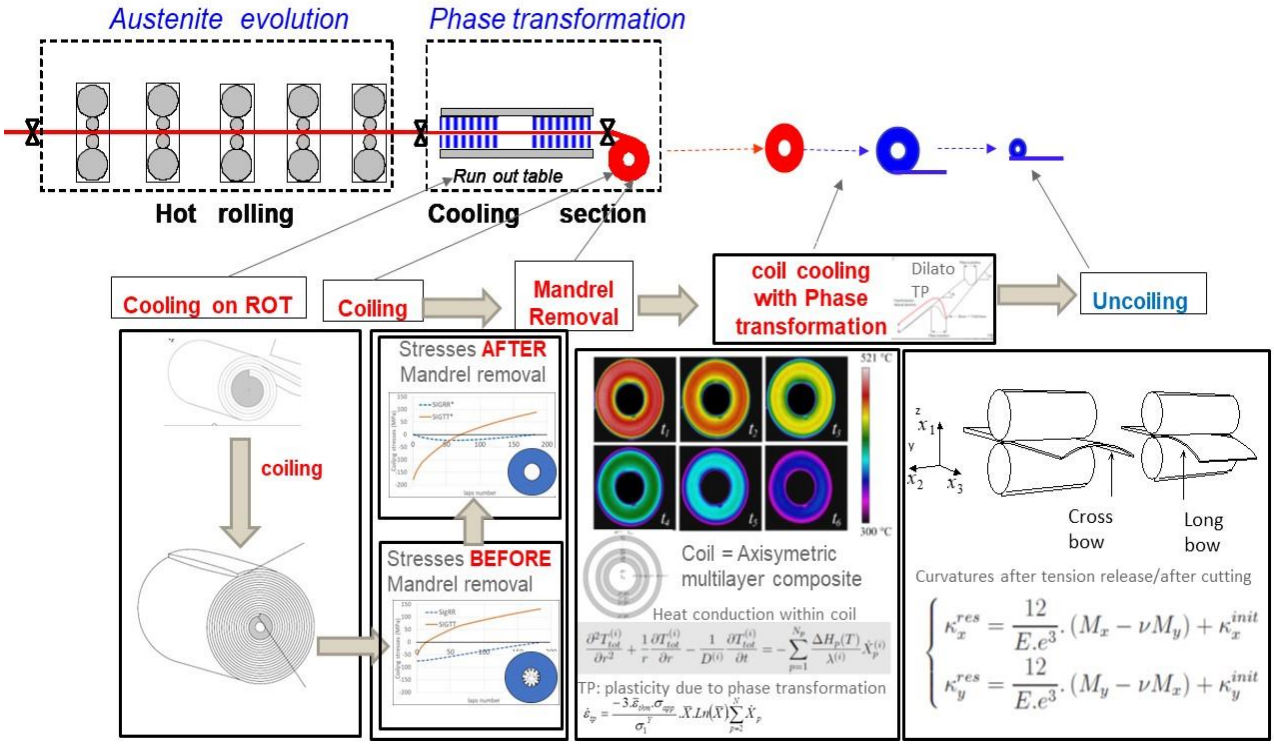


**Fig.17** The thermo-mechanical coil cooling model combining several sub models (models 1 and 2)

**Simulation conditions:**

Model 1: **Temperature and phase transition model**
First the model [4] is exploited with process parameters listed in table 6 to simulate the temperature evolution over time during the entire process (i.e., run out table, coiling and coil cooling processes). The multiphase transformation kinetics Avrami and Koistinen model calibrated previously on grades A and B is then used to compute the phase proportion within the entire coil for grades A and B after the mandrel is removed. Process parameters are listed in table 5, and material properties are listed in table 6. No particular tuning on measured temperatures is made with this model, a general tuning from previous analysis is re-used here.

Model 2: **Contact pressure dependent model** (thermomechanical model)
After mandrel removal, slow coil cooling takes place, which not only depends on material parameters, boundary conditions, coil geometry and phase transitions, but also on heterogeneous contact pressures between laps, which is not taken into account in model 1 [4]. Therefore, a specific coil cooling model proposed in [10] is also used in combination with mechanical models proposed in [7], [8] to obtain a more detailed estimation of temperature kinetics and phase transition during the slow cooling of the coil after mandrel removal which accounts for heterogeneous contact pressures. This thermo-mechanical model has also ability to predict residual stress evolution in the coil during coil cooling (ability not exploited in the present paper but planned to be exploited in future works).

**Table 5:** Process parameters and thermal boundary conditions for coil cooling simulations – grades A and B

| | Grade A (coil 2) | Grade B (coil 1) |
|---|---|---|
| Number of laps | 164 | 168 |
| Strip width (mm) | 1163 | 1187 |
| Strip thickness (mm) | 2.98 | 2.92 |
| Strip length (meter) | 636 | 642 |
| Coiling Tension at coiler (MPa) | 36 (MPa) 1st half of laps, 21.74 (MPa) 2nd half, 0 (MPa) last few laps | |
| Mandrel diameter (mm) | 750 | 750 |
| Average strip crown (mm) | 0.025 | 0.038 |
| Time between end of coiling and mandrel removal (sec.) | 50 | 25 |
| Mandrel initial temperature (celcius) | 60 | 60 |
| Thermal contact transmittance between laps (W/mm2.K) | 625.e-6 | 625.e-6 |
| Thermal contact transmittance between lap1 and mandrel (W/mm2.K) | 909.e-6 | 909.e-6 |
| Heat Transfer Coefficient Convection outer lap/air (W/mm2/K) | 8.e-6 | 8.e-6 |
| Heat Transfer Coefficient Convection inner lap-air (W/mm2/K) | 8.e-6 | 8.e-6 |
| Heat Transfer Coefficient Convection edge-air (W/mm2/K) | 8.e-6 | 8.e-6 |
| Radiation coefficient outer lap-air | 1 | 1 |
| Radiation coefficient inner lap-air | 0 | 0 |
| Radiation coefficient edge-air | 1 | 1 |

**Table 6:** Material properties for coil simulation – coil 1 grade B

| | |
|---|---|
| Young modulus | 202174 (MPa) – 87 (MPA/K) ×$T$ (K) |
| Poisson modulus | 0.3 |
| Thermal conductivity of steel | 50 ×$10^{-3}$ (W.mm$^{-1}$.K$^{-1}$) |
| Thermal conductivity of air | 0.026 ×$10^{-3}$ (W.mm$^{-1}$.K$^{-1}$) |
| Thermal diffusivity of steel | 12 (mm$^2$.s$^{-1}$) |
| Thermal diffusivity of air | 20 (mm$^2$.s$^{-1}$) |
| Heat transfer coefficient between coil and surrounding air | $10^{-5}$ (W.mm$^{-2}$.K$^{-1}$) |
| External temperature | 293 (K) |
| Heat transfer coefficient between laps | 150 to 1100 (W.mm$^{-2}$.K$^{-1}$) |

It should be noted that a perfect contact condition is implemented during coiling in [7], [8] (in which a continuous orthotropic body is considered for the coil instead of a multi-lap structure), thus the coiling simulation tends to

overestimate the barrel shape of the coil. To compensate this effect the strip crown is set to 0.001 mm following [25]). Resulting contact pressures are then updated at the end of coiling when the mandrel is removed (i.e., imposing a free boundary condition at the inner radius of the coil) by using an iterative algorithm to compute a non-linear multilayer problem similar to [11] with a contact law accounting for roughness between each layer (i.e., penalization of nominal surfaces). In addition, volume change due to thermal expansion and phase transitions during the coiling step (i.e., difference between the strip temperature at the coiler and just before removing the mandrel) is applied. However, it should be noted that this step is done under a 1D assumption (i.e., radial direction), which does not enable to capture possible bending of outer and inner laps due to thermal shrinkage along both the radial and axial directions as illustrated on figure 16-a. Numerical results clearly show that this 1D assumption (in the computation of contact pressures when the mandrel is removed) leads to inaccurate contact pressure distribution at the edge of the coil. Indeed, even though the interpenetration of nominal surfaces during mandrel removal are consistent for a large part of the coil with the experimental observations of the stacking of laps (i.e., gaps between laps for inner and outer laps and tight contact with no/small gap for the central laps), the computed interpenetration remains negative with a tight contact for outer laps while observations provide evidence of the opposite. This model limitation has to be overcome in future works by performing 3D computations for the contact pressure estimation. In this paper though, to mitigate this issue, a contact pressure distribution consistent with the observations of loose laps for inner and outer zones is postulated at the coil edge so that further temperature fields are correctly captured (figure 18). It should be noted that contact pressures are not modified for the rest of the coil.
In addition, the model proposed in [10] was developed by neglecting heat fluxes along the coil axis, which had to be introduced in the present contribution (by using an additional analytical solution similar to the already existing analytical solutions proposed in [10]) as infrared measurements on the front and side views clearly show that heat fluxes along the axial direction cannot be neglected.

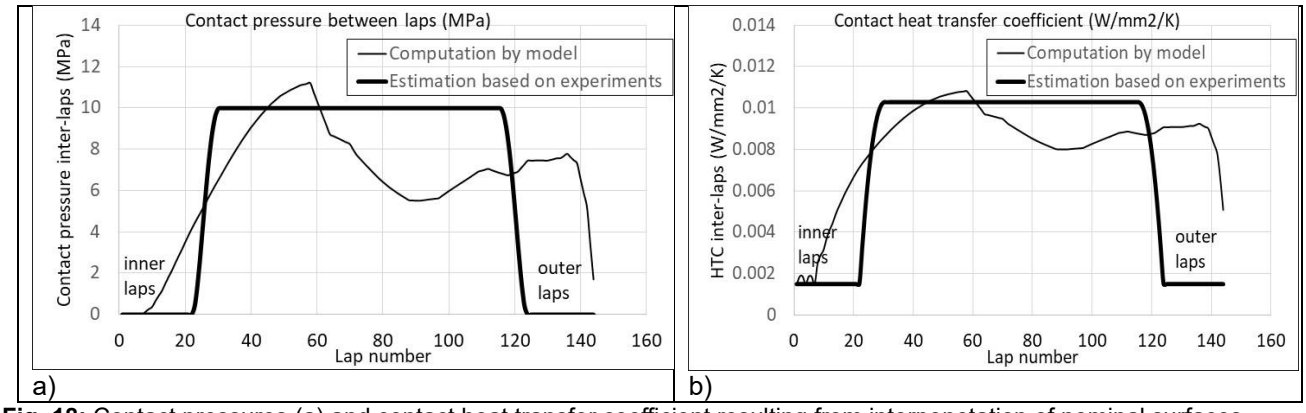


**Fig. 18:** Contact pressures (a) and contact heat transfer coefficient resulting from interpenetation of nominal surfaces (simulated and estimated from direct observation during trials) – model 2-

**Simulation results:**

A series of simulation results and comparisons with coil temperature measurements (front view) are provided below for the two grades. The goals are to compare and analyze the coil cooling kinetics of the two grades and identify the necessary improvements to implement in the coil cooling simulation tools.

Model 1 simulation results: **Temperature and phase transition model**

The temperature predictions obtained with the model from [4] and [5] are compared with the measured temperatures from cameras for coils 2 (grade A) and coil 1 (grade B). The comparison presented on figure 19 for coil 2 (grade A) shows that the model predictions are acceptable (no particular tuning was made in this comparison, the model tuned from previous trials was used here). However, this tuning can be improved. This is the objective of the next sections. Nevertheless, even though predictions are not perfect with the original model 1, these first computations enable to roughly evaluate the time-temperature cooling path of the strip during its travel on the run-out table, coiling and coil cooling and compare the two grades with respect to their CCT and TTT diagrams (figures 20 and 21). In figure 20, by comparing CCT diagrams one can observe that

grade A at coiler has almost no austenite transformed yet (almost all transformation will happen in the coil). While with grade B, the transformation has already started. This shows once again that grade A is coil transforming while grade B is more run out table transforming or both. In figure 21, by comparing TTT diagrams, same conclusions are obtained: grade A at coiler has not yet started the transformation while grade B has. More importantly, the TTT diagram reflecting the bay (delay to transformation), figure 21-b also shows that grade B central laps avoid for most of the part this bay (because of shorter bay and bay at lower temperature; while figure 21-a shows that coil cooling of grade A (central laps) tends to happen in the bay for the edges of central laps while for central laps middle width, the bay is avoided. This difference between edges and center line may be one source of twist shape defect for grade A but further analysis is needed.

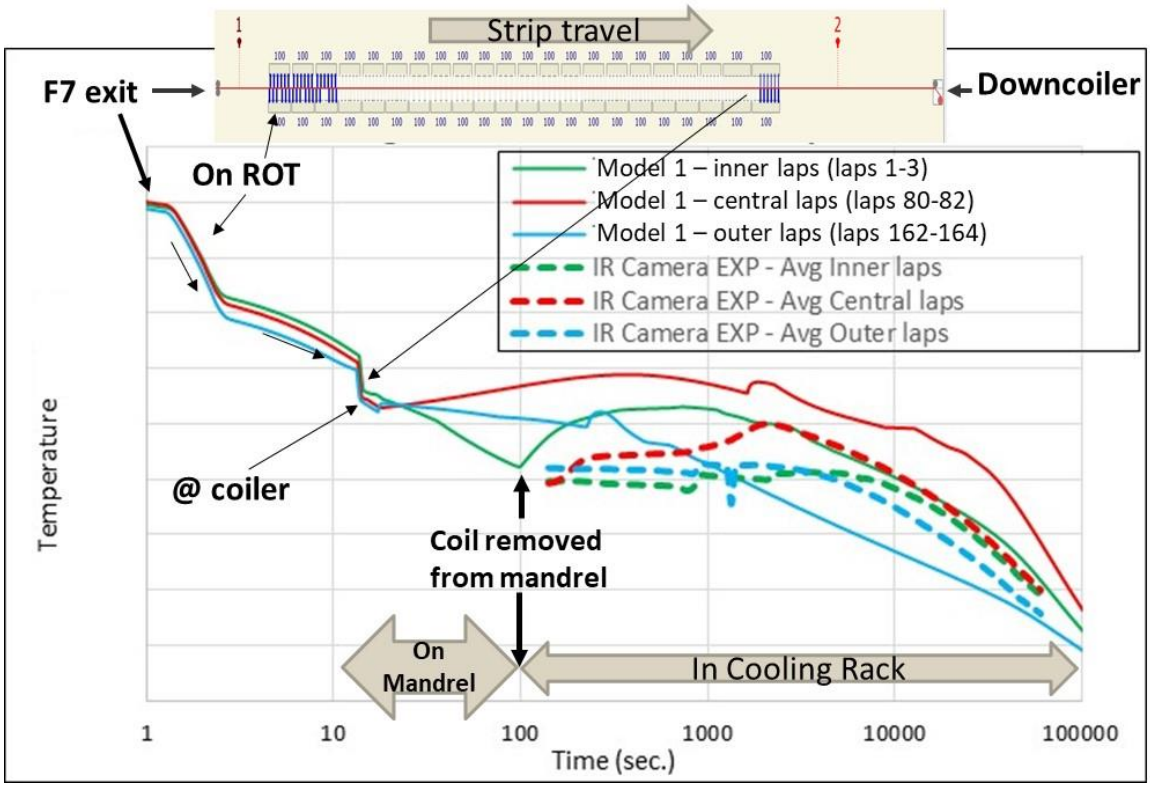


**Fig. 19:** Time-temperature cooling path measured and calculated by model 1 – coil 2 grade A (no specific tuning was made for this comparison)

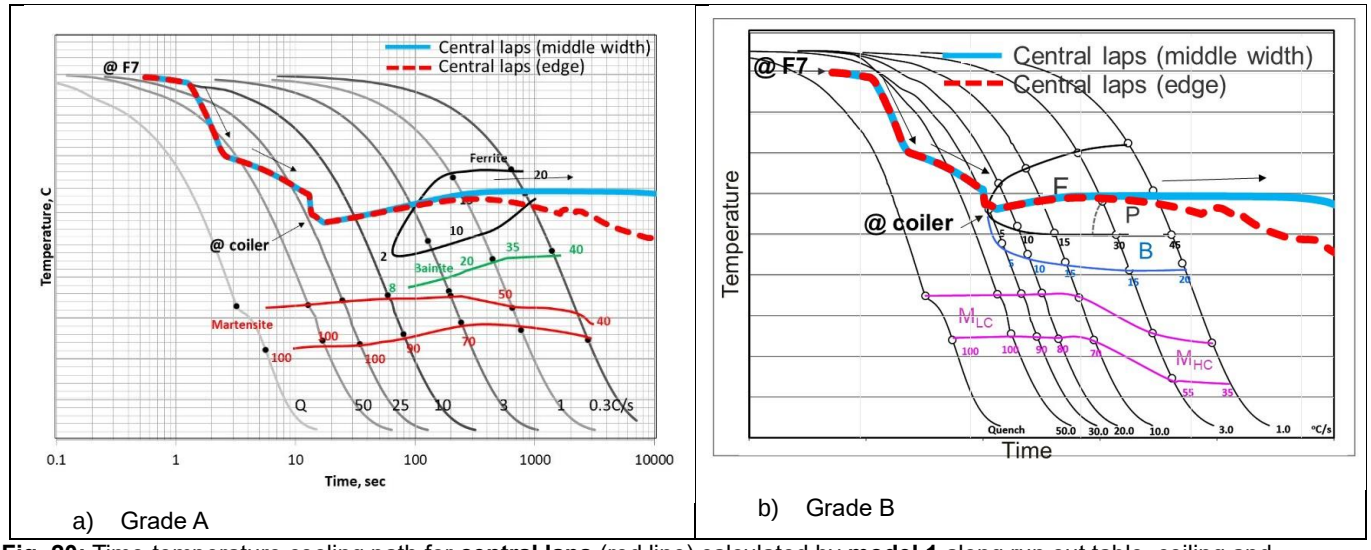


**Fig. 20:** Time-temperature cooling path for **central laps** (red line) calculated by **model 1** along run out table, coiling and coil cooling processes for a) grade A and b) grade B. Comparison with **CCT diagrams**.

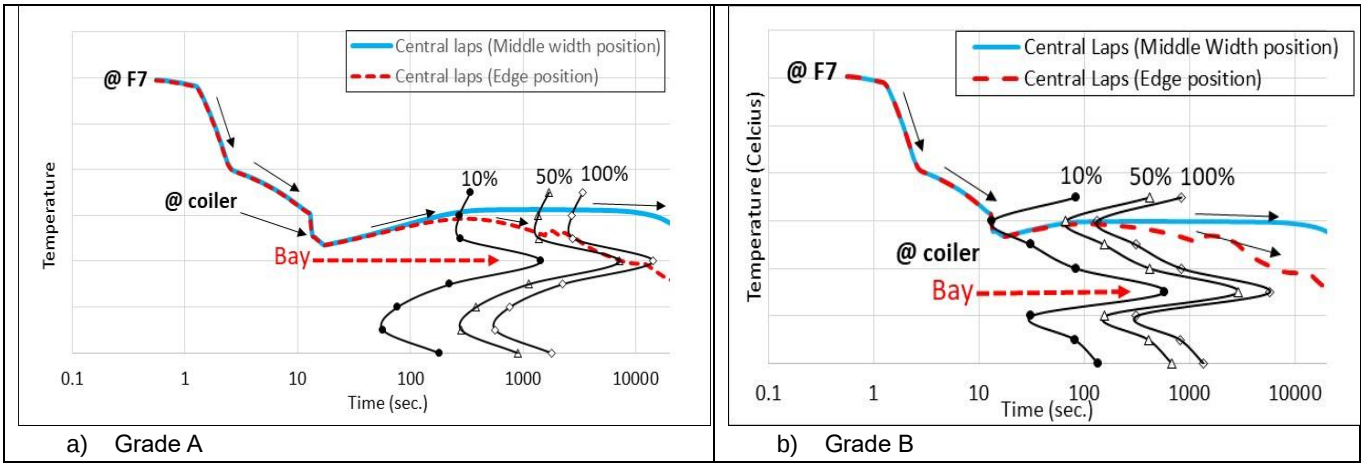


a) Grade A b) Grade B

**Fig. 21:** Time-temperature cooling path in the central laps middle width (center line) & edge calculated by **model 1** along run out table, coiling and coil cooling processes for a) grade A and b) grade B. Comparison with **TTT diagrams**.

The initial temperatures are set at mandrel removal, which are extracted from the previous simulation using model 1 [4], [5] (figure 22-a), and the corresponding phase fractions are obtained by using the calibrated Avrami and Koistinen equations (figure 22-b). Grade A is mostly austenitic when the mandrel is removed, which leads to further important phase transition during coil cooling, while grade B is already entirely decomposed into ferrite+pearlite and bainite.

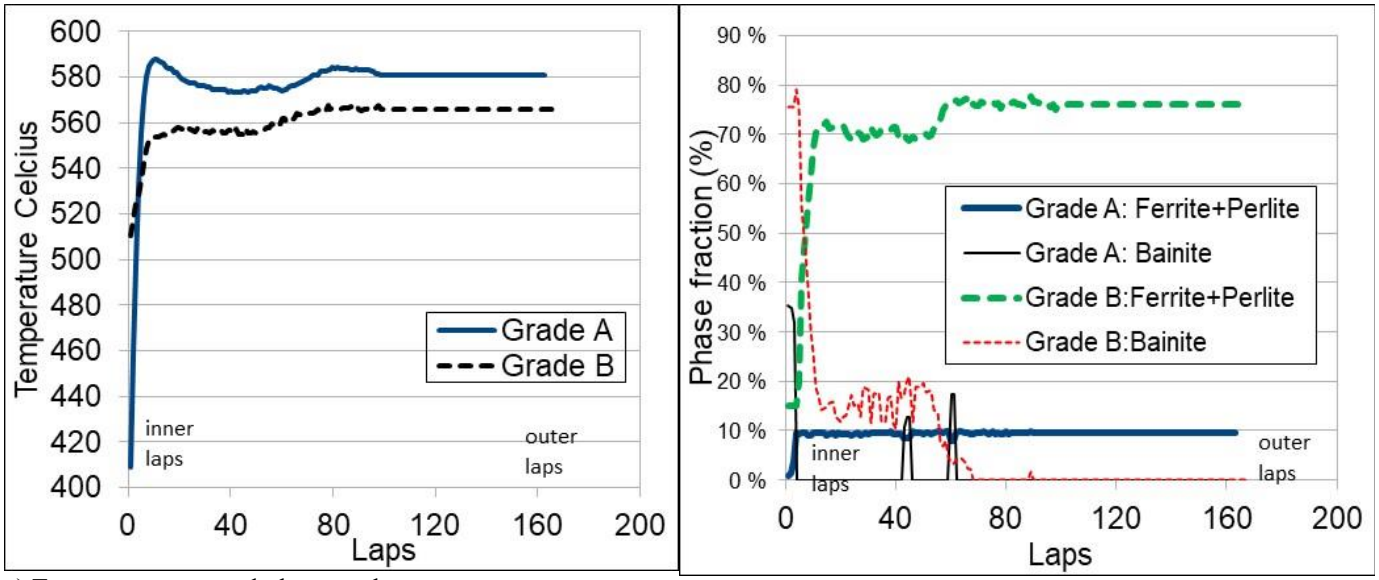


a) Temperature at mandrel removal b)Phase fractions at mandrel removal

**Fig. 22:** a) Temperature and b) phase proportions at mandrel removal at the coil edge computed with models 1 for both grades A and B. Initial temperatures predicted by model 1.

Model 2 simulation results: **contact pressure dependent model**

A comparison with infrared measurements of the improved contact dependent coil cooling model (model 2) is provided in figure 23. A reasonable agreement model-experiments is obtained for both front and side views, which enables us to use the model to compute phase transitions in the entire coil for both grades.

However, it is seen at t = 0 seconds (mandrel removal) that computed and measured outer lap temperatures significantly differ from each other's (purple curve). It is believed that this difference is due to the massive volume of water sprayed on the coil just before mandrel removal (e.g., after end of coiling), which significantly cools down the outer lap (this water cooling is not explicitly considered in the tuning of the present model).

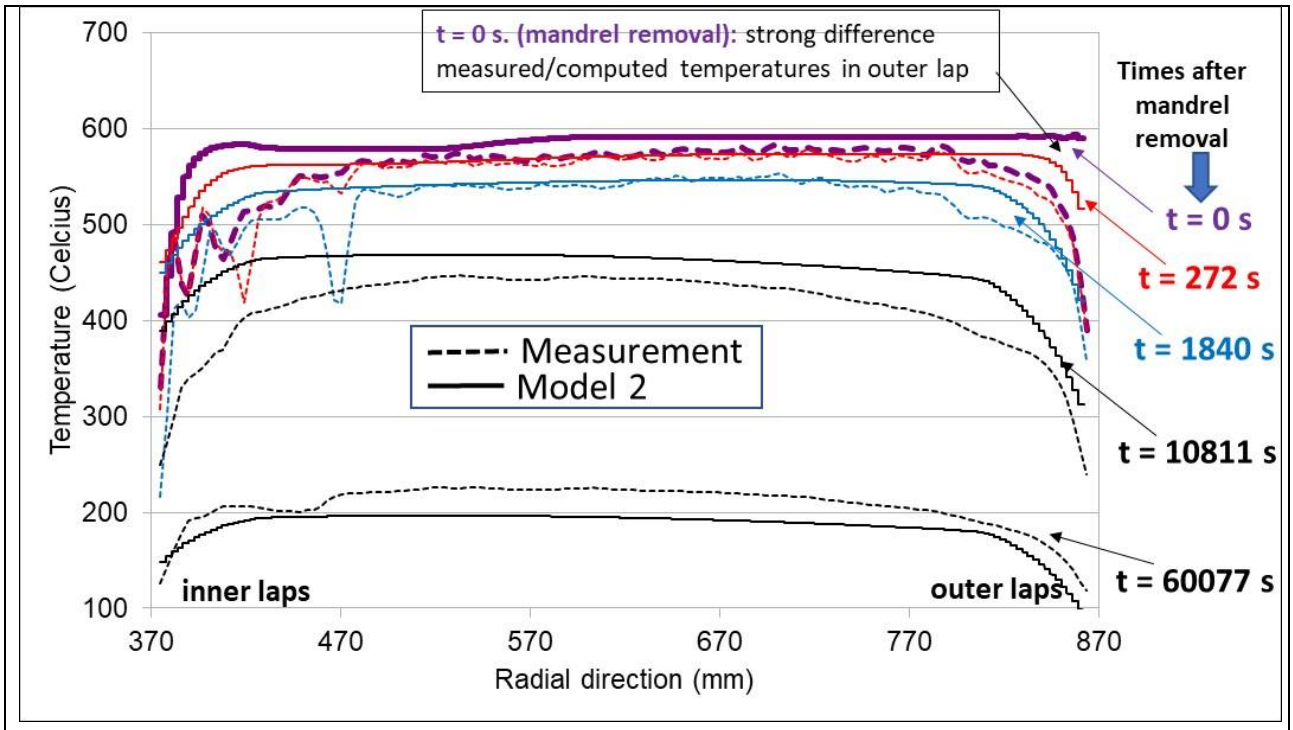


a) Front view

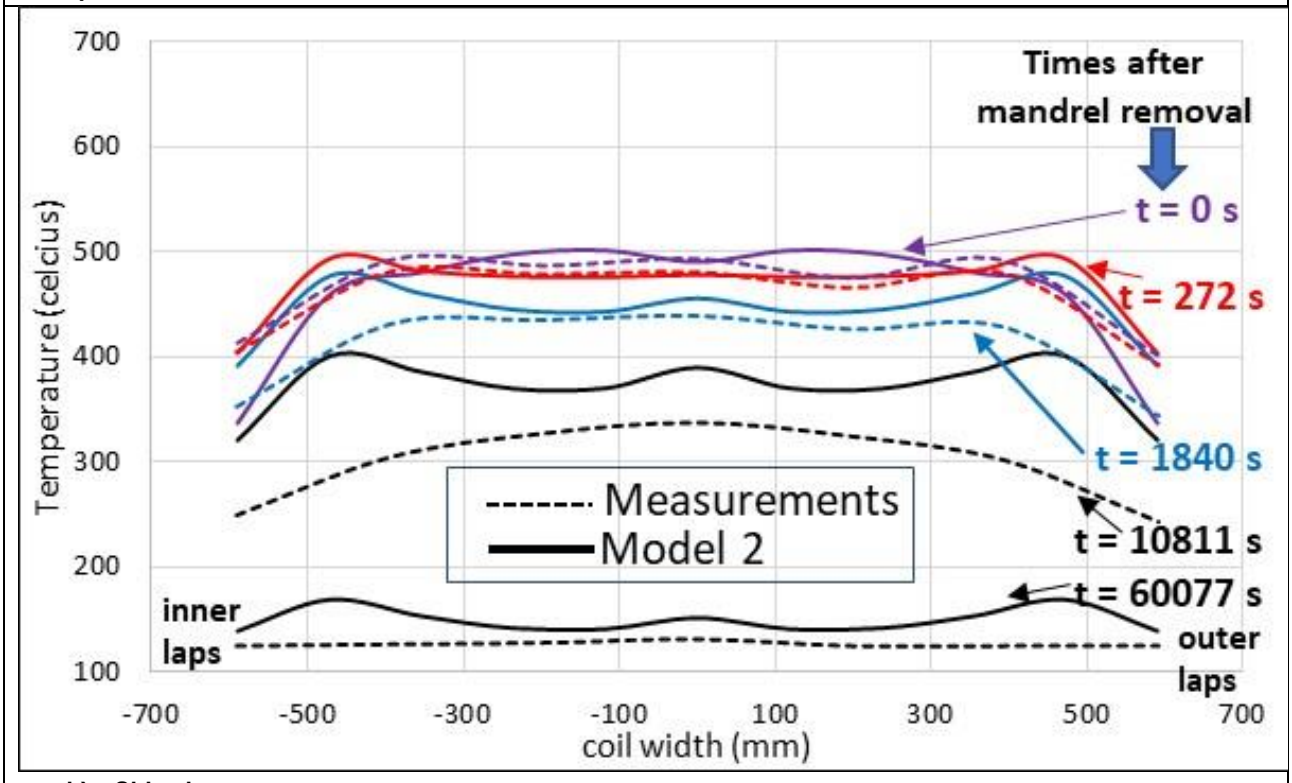


b) Side view

**Fig. 23:** Comparison between measured and computed temperatures for different cooling times as a function of: a) radial position at coil edge (Front view) b) axial position (width) side view – grade B coil 1 - model 2 –

The total amount of produced phase during coil cooling (i.e., ferrite+pearlite+bainite+martensite) is presented as a function of time at the coil edge for both grades in figure 24-a. Similar results are obtained at the coil center. One can observe that since grade A does not transform on the run out table, most of the phase transition occurs during coil cooling while the opposite is observed for grade B. Combined with bending stresses in the laps in the coiled coil (figure 24-b), this leads to significant volume change and transformation induced plasticity in grade A, particularly near ID area, which leads to residual stresses and flatness issues in the coil ID.

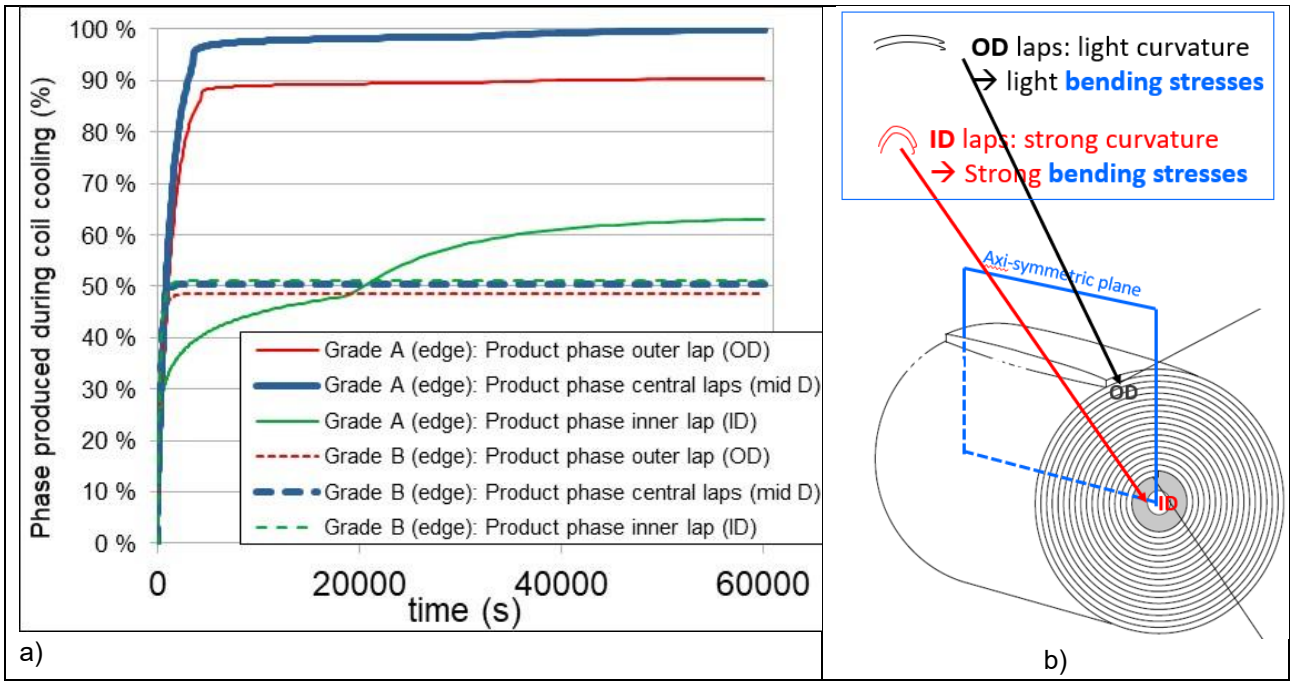


**Fig. 24:** The two mechanisms responsible for twist shape issues of grad A: a) Produced phase during coil cooling (since mandrel removal, for three different laps) more important for grade A – model 2- b) bending stresses stronger in coil ID

In addition, the distribution of martensite for the first laps (i.e., ID) is presented in figure 25 for grade A: results are consistent with hardness measurements in figure 5. However, the model predicts no martensite for grade B while microstructure analysis on metallography and hardness measurements (figure 6) indicates the presence of martensite. This disagreement with observations needs further analysis and model improvements.

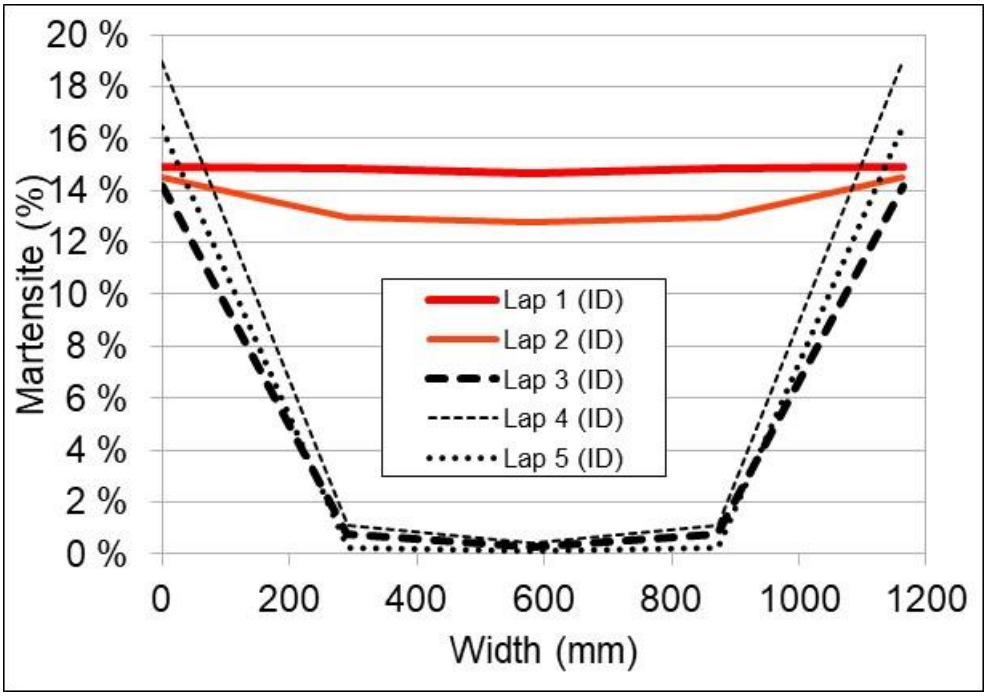


**Fig. 25: Grade A** Martensite distribution as a function of width at ID – model 2-

## NEW ROLLING PRACTICES APPLICATION: INDUSTRIAL RESULTS

Twist shape issue (grade A):

Based on the previous analysis, in order to mitigate the twist shape issue, the coil cooling model has been used to maximize phase transformation on the run out table by changing finishing and by minimzing residual stresses in the coil. These modifications (not detailed here) have been applied to the mill and have generated positive results in terms of yield loss and crop length decrease (figure 26).

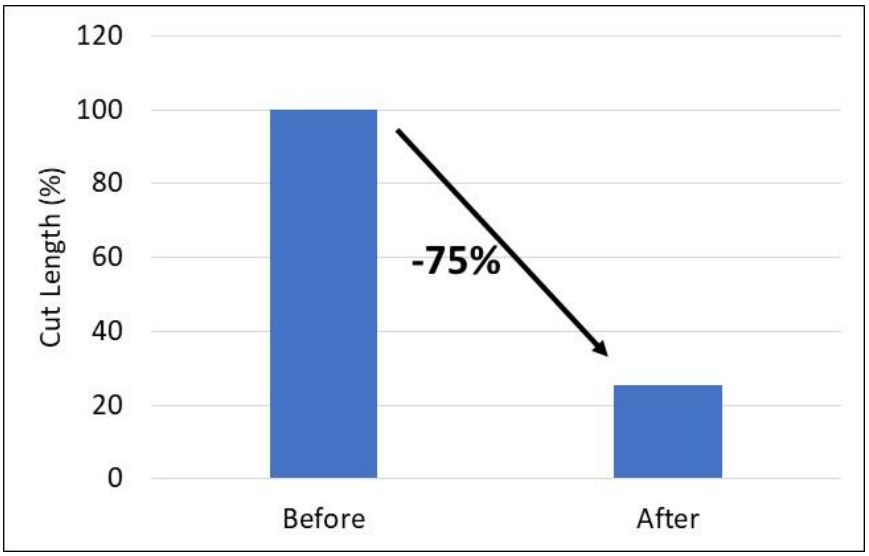


**Fig. 26: Grade A** Yield loss before and after maximizing the phase transformation on the run out table (e.g. minimizing phase transformation in the coil) and by homogeneizing residual stress formation.

Hardness variability issue (grade B):

Based on the previous analysis, in order to mitigate the hardness variability issue at coil extremities, the coil cooling model has been used to evaluate an increase of coiling temperature at head and tail of grade B. Figure 27 shows that such an increase of coiling temperature could limit martensite hard phase formation because it maintains head a longer time in ferrite-pearlite areas so forms more soft phases so less hard phases in subsequent cooling.

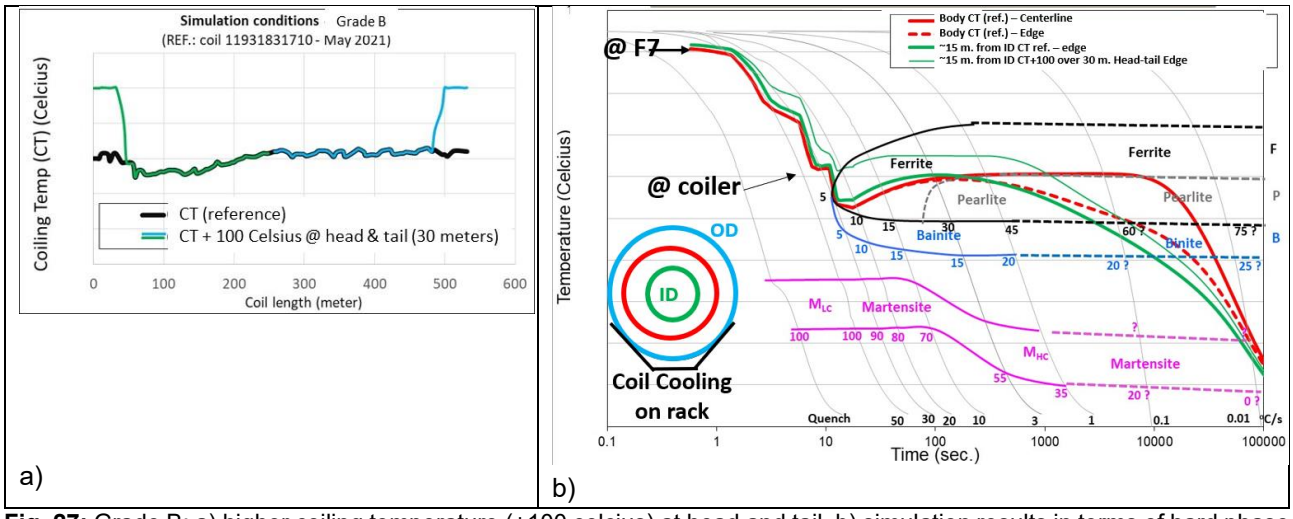


**Fig. 27:** Grade B: a) higher coiling temperature (+100 celcius) at head and tail. b) simulation results in terms of hard phase formation (martensite) at extremities: reference (uniform coiling temperature) versus hot head and tails.

Industrial trials were conducted on the mill with these warmer coiling temperatures at extremities; but did not show any major improvement in hardness variability issues (results not shown here): this coiling temperature increase is not sufficient to compensate for the heat losses of extremities. Further modeling analysis and trials are needed.

## CONCLUSIONS

### Coil cooling model improvement and calibration:

The present work has developed a methodology to tune an existing coil cooling model after hot rolling and applied the tuned model to better understand manufacturability issues (twist shape and hardness variability) of two different high strength steel grades A and B:

- Three infrared cameras have been used to capture the temperature evolution during coil cooling.
- Phases transitions have been modeled by Avrami and Koistinen equations tuned on dilatometric tests.
- The temperature field history of the coil has been computed by a series of previously developed simulation tools: temperature, phase transition and mechanical state during run out table coiling and coil cooling processes.

The experiments have been used to estimate the validity of the numerical approach used in the existing simulation tools. Indeed, these theoretical models rely on severe assumptions to reduce computation time, but still needed experimental evidences. Results show that numerical simulations have to be improved. After several improvements detailed in the paper, a good agreement has been finally obtained between model predictions and coil temperature measurements by infrared cameras (i.e., slow cooling after mandrel removal). On this basis phase proportions evolution and the evolution of residual stresses during cooling can be computed using existing models.

### Coil cooling model exploitation:

The model together with experiments have then been used to better understand the two grades issues. First it has been shown/confirmed by several different experimental and modeling analysis that grade A is a coil transforming grade while grade B is more a run out table transforming grade:

- the transformation in the coil combined with the bending stresses stronger in the laps near the mandrel are the prime source of the twist shape for grade A.
- grade B does not have twist shape issue because of sufficient transformation happening on the run out table before coiling and coil cooling.
- There are several reasons why grade A is coil transforming and grade B is more run out table transforming:
    - Grade A presents a long bay (delay to transformation) that is close to the coiling temperature of this grade: this naturally favor transformation in the coil.
    - Grade B presents a shorter bay appearing at a lower temperature, that is noticeably lower than the coiling temperature: this avoids/limits transformation in the coil.
    - Grade B phase transformation start is more sensitive than grade A to austenite plastic deformation in hot rolling, this favors even more transformation in the run out table for grade B. The reason of this difference is due to a difference of chemistry between the two grades that cannot be disclosed here due to confidentiality.

## REFERENCES

[1] Montmitonnet, P. (2006). Hot and cold strip rolling processes. *Computer methods in applied mechanics and engineering*, *195*(48-49), 6604-6625.

[2] Hacquin, A. (1996). *Modelisation thermomecanique tridimensionnelle du laminage couplage bande/cylindres* (Doctoral dissertation, Paris, ENMP).

[3] Iung, T., Kandel, M., Quidort, D., & De Lassat, Y. (2003). Physical modelling of phase transformations in high strength steels. *Metallurgical Research & Technology*, *100*(2), 173-181.

[4] Perlade, A., Grandemange, D., & Iung, T. (2005). Application of microstructural modelling for quality control and process improvement in hot rolled steels. *Ironmaking & steelmaking*, *32*(4), 299-302.

[5] Jacolot, Ronan, Didier Huin, Artem Marmulev, and Eliette Mathey. “Hot Rolled Coil Property Heterogeneities Due

to Coil Cooling: Impact and Prediction." Key Engineering Materials. Trans Tech Publications, Ltd., September 2014

[6] Weisz-Patrault, D., & Koedinger, T. (2018). Residual stress on the run out table accounting for multiphase transitions and transformation induced plasticity. *Applied Mathematical Modelling*, *60*, 18-33.

[7] Weisz-Patrault, D., Ehrlacher, A., Legrand, N., & Mathey, E. (2015). Non-linear numerical simulation of coiling by elastic finite strain model. In *Key Engineering Materials* (Vol. 651, pp. 1060-1065).

[8] Weisz-Patrault, D., & Ehrlacher, A. (2017). Imposed curvature of an elastic-plastic strip: application to simulation of coils. *Mechanics & Industry*, *18*(2), 218.

[9] Weisz-Patrault, D., Ehrlacher, A., & Legrand, N. (2016). Non-linear simulation of coiling accounting for roughness of contacts and multiplicative elastic-plastic behavior. *International Journal of Solids and Structures*, *94*, 1-20.

[10] Weisz-Patrault, D. (2017). Coupled heat conduction and multiphase change problem accounting for thermal contact resistance. *International Journal of Heat and Mass Transfer*, *104*, 595-606.

[11] Weisz-Patrault, D. (2018). Nonlinear and multiphysics evaluation of residual stresses in coils. *Applied Mathematical Modelling*, *61*, 141-166.

[12] Weisz-Patrault, D., Gantier, M., & Ehrlacher, A. (2019). Mixed analytic/energetic approach for a sliding orthotropic hollow cylinder. Application to coil sagging. *International Journal of Solids and Structures*, *165*, 75-92.

[13] Weisz-Patrault, D., Ehrlacher, A., & Legrand, N. (2011). A new sensor for the evaluation of contact stress by inverse analysis during steel strip rolling. *Journal of Materials Processing Technology*, *211*(9), 1500-1509.

[14] Weisz-Patrault, D., Ehrlacher, A., & Legrand, N. (2013). Evaluation of contact stress during rolling process, by three dimensional analytical inverse method. *International Journal of Solids and Structures*, *50*(20-21), 3319-3331.

[15] Weisz-Patrault, D., Maurin, L., Legrand, N., Salem, A. B., & Bengrir, A. A. (2015). Experimental evaluation of contact stress during cold rolling process with optical fiber Bragg gratings sensors measurements and fast inverse method. *Journal of Materials Processing Technology*, *223*, 105-123.

[16] Weisz-Patrault, D., Ehrlacher, A., & Legrand, N. (2012). Evaluation of temperature field and heat flux by inverse analysis during steel strip rolling. *International Journal of Heat and Mass Transfer*, *55*(4), 629-641.

[17] Weisz-Patrault, D., Ehrlacher, A., & Legrand, N. (2014). Temperature and heat flux fast estimation during rolling process. *International Journal of Thermal Sciences*, *75*, 1-20.

[18] Legrand, N., Labbe, N., Weisz-Patrault, D., Ehrlacher, A., Luks, T., & Horský, J. (2012). Analysis of roll gap heat transfers in hot steel strip rolling through roll temperature sensors and heat transfer models. In *Key Engineering Materials* (Vol. 504, pp. 1043-1048).

[19] Legrand, N., Weisz-Patrault, D., Horský, J., Luks, T., Labbe, N., Picard, M., & Ehrlacher, A. (2013). Characterization of roll bite heat transfers in hot steel strip rolling and their influence on roll thermal fatigue degradation. In *Key Engineering Materials* (Vol. 554, pp. 1555-1569).

[20] Weisz-Patrault, D., Ehrlacher, A., & Legrand, N. (2013). Analytical inverse solution for coupled thermoelastic problem for the evaluation of contact stress during steel strip rolling. *Applied Mathematical Modelling*, *37*(4), 2212-2229.

[21] Weisz-Patrault, D. (2015). Inverse cauchy method with conformal mapping: application to latent flatness defect detection during rolling process. *International Journal of Solids and Structures*, *56*, 175-193.

[22] Weisz-Patrault, D. (2017). Multiphase model for transformation induced plasticity. Extended Leblond's model. *Journal of the Mechanics and Physics of Solids*, *106*, 152-175.

[23] Avrami, M. (1941). Granulation, phase change, and microstructure kinetics of phase change. III. *The Journal of chemical physics*, *9*(2), 177-184.

[24] Koistinen, D. P. (1959). A general equation prescribing the extent of the austenite-martensite transformation in pure iron-carbon alloys and plain carbon steels. *Acta metallurgica*, *7*, 59-60.

[25] Joonas Ilmola et al, Coupled heat transfer and phase transformations of dual-phase steel in coil cooling, Materials Today Communications, 2021.

[26] Internal communication ArcelorMittal – O. Girina

[27] Internal communication ArcelorMittal – M. Tavassoly

**Acknowledgements**

William Umlauf, Jim Uram and Olga Girina from ArcelorMittal East Chicago Research are greatly acknowledged respectively for their help in supporting and preparing industrial coil cooling trials, performing dilatometric tests and evaluating phase fractions by metallography on the dilatometric samples for grades A and B for CCT diagrams.

A. Wagatsuma, M. Parson and M. Peacock from AMNS Calvert are greatly acknowledged for assistance during the industrial trials.